RNA decay defines the therapeutic response to transcriptional perturbation in cancer

Izabela Todorovski[1,2], Breon Feran[3,4], Zheng Fan[1,2], Sreeja Gadipally[1], David Yoannidis[1], Isabella Y Kong[3,4], Edwin D Hawkins[3,4], Kaylene J Simpson[1,2], Gisela Mir Arnau[1,2], Anthony T Papenfuss[1,2,3,4], Ricky W Johnstone[1,2,] †*, Stephin J Vervoort[1,2,3,4]†*

[1]Peter MacCallum Cancer Centre, Melbourne, Victoria 3000, Australia

[2]Sir Peter MacCallum Department of Oncology, The University of Melbourne, Victoria 3010, Australia

[3]The Walter and Eliza Hall Institute of Medical Research, Parkville, Australia.

[4]Department of Medical Biology, The University of Melbourne, Parkville, Australia.

†Co-senior authors.

*Corresponding authors. Email: vervoort.s@wehi.edu.au, ricky.johnstone@petermac.org

ABSTRACT

Transcriptionally dysregulated cancers are sensitive to the inhibition of RNA Polymerase II (RNAPII) - driven gene expression. The therapeutic effect is attributed to selective inhibition of discrete oncogenes regulated at the chromatin level, however the role of RNA stability remains largely unexplored. Using integrated transcriptomic technologies, we discovered that RNA decay is a key determinant in defining gene expression responses to transcriptional perturbation, where total RNA signatures are dominated with genes that have short transcript half-lives, including oncogenic drivers such as *c-MYC*. Experimentally increasing *c-MYC* RNA stability maintained total *c-MYC* RNA levels following RNAPII perturbation, despite a concordant decrease in nascent RNA. Taken together, these data demonstrate that RNA decay shapes the molecular and therapeutic response to transcriptional perturbation in cancer.

HIGHLIGHTS

- Selective inhibition of oncogenic transcription in response to epigenetic and transcriptional inhibitors in cancer under-estimates the role of RNA decay
- Gene intrinsic RNA decay rates are a key determinant in shaping the total mRNA response to transcriptional perturbation in cancer
- Selective disruption of core-transcription factor networks is a result of short transcript half-lives
- Modulation of c-MYC decay rates can render it insensitive to transcriptional targeting

INTRODUCTION

Genetic alterations in cancer can affect proteins involved in almost all regulatory steps of RNA Polymerase II (RNAPII) -driven transcription, including histones, transcription factors (TFs), epigenetic enzymes and reader proteins, chromatin remodelers and RNAPII itself [1]. These changes dysregulate transcription and ultimately contribute to cellular transformation and the development malignant phenotypes [1,2].

Transcriptionally dysregulated cancers exhibit a critical dependency on components of the core transcription machinery that regulate RNAPII-driven gene expression, a notion termed 'transcription addiction' [1]. This has spurred the development of small molecule inhibitors that target core transcriptional enzymes and structural proteins for therapeutic benefit [3,4]. For example, displacement or degradation of the Bromodomain and Extra Terminal (BET) family of epigenetic reader proteins such as Bromodomain-Containing Protein 4 (BRD4) has demonstrated pre-clinical efficacy across solid and hematological malignancies [5–13]. Moreover, perturbation of the histone acetyltransferase activity of the transcriptional co-activator p300/cAMP-response element binding protein (CBP) with A-485 reduced the proliferation of androgen receptor (AR) -positive prostate cells and provided therapeutic benefit in pre-clinical studies [14]. In addition to disrupting the epigenetic control of transcription, the productive cycling of RNAPII through initiation, elongation and termination can be prevented by inhibition of transcriptional Cyclin Dependent Kinases (t-CDKs) and steric hinderance via DNA-intercalating agents like Actinomycin D (ACTD) [15,16]. Targeting of the t-CDK, CDK9, reduced tumor load in pre-clinical models of Mixed Lineage Leukaemia (MLL) -driven Acute Myeloid Leukemias (AMLs) and MYC-amplified malignancies [15,17,18]. Notably, the CDK9 inhibitor BAY1251152, is currently in phase I clinical trials in advanced solid neoplasms [19]. In contrast, ACTD is already a widely used chemotherapy agent for Ewing's sarcoma, rhabdomyosarcoma and Wilm's tumor [19].

Therapeutic inhibition of RNAPII-driven gene expression has been proposed to elicit selective transcriptional responses. A current model suggests that this selectivity is associated with particular genomic elements such as super-enhancers (SEs), which are large collections of enhancers that exhibit high occupancy of cell type specific transcription factors (TFs), p300/CBP and BRD4 among other epigenetic co-factors [20]. For example, JQ1 treatment in models of Multiple Myeloma (MM) disproportionately downregulated key SE-associated MM-driver genes in comparison to typical enhancers via the displacement of BRD4 [21]. This was similarly observed with the t-CDK7/12/13 inhibitor THZ1, whereby oncogenes and TFs associated with SEs were uniquely sensitive in MYC-amplified neuroblastoma, Small Cell Lung Cancer (SCLC) and T-cell Acute Lymphoblastic Leukaemia (T-ALL) [22–24]. In contrast, CDK9 inhibitors can globally affect transcription to varying degrees by perturbating early elongation and polyadenylation (polyA) checkpoints, with apoptotic regulatory genes such as *MCL-1* and *XIAP* proposed to be selectively downregulated [19,25]. Similarly, gene expression is broadly inhibited with ACTD treatment [16,19].

Conventional RNA profiling techniques that measure total RNA abundance are routinely used to assess gene expression. However, this precludes any differences in intrinsic RNA production and decay rates that might influence changes in expression. Recent technological advances have enabled the measurement of nascent RNA and its decay over time. Metabolic labelling of RNA with the nucleotide analog 4-thiouridine (4sU), and its quantification using affinity- or conversion-based technologies, represents the most widely used

approach to track an RNA species over time without affecting cellular integrity [26-31]. For example, thiol (SH)-linked alkylation for the metabolic sequencing of RNA sequencing (SLAM-seq) is a conversion-based approach that uses 4sU dependent thymine-to-cytosine (T > C) conversions for the *in silico* separation of newly synthesized and pre-existing transcripts [26]. Indeed, assessment of transcriptional responses to BRD4 and CDK9 inhibition in pre-clinical models of leukaemia using SLAM-seq revealed a global decrease in nascent RNA that was not recapitulated in the total RNA pool [32]. Although the nascent gene response to BRD4 inhibition was well predicted by various chromatin factors occupying the transcription start site (TSS) of downregulated genes, such as *c-MYC* and *PIM1* [32], the role of RNA decay in affecting global changes in total RNA expression in cancer is yet to be explored.

Here, we used SLAM-seq to assess the role of RNA decay in shaping gene expression responses to the therapeutic targeting of different transcriptional regulatory components. Genes with short lived transcripts were the most prominent in RNA signatures derived upon global transcriptional perturbation. Small molecule inhibition of t-CDKs and the general RNAPII machinery, resulted in gene expression changes that could most strongly be predicted by transcript half-lives alone. Using this information, we demonstrated that stabilization of the *c-MYC* transcript through re-engineering of the 3' untranslated region (UTR) was sufficient to render it less sensitive to global transcriptional inhibition. Taken together, we provide a novel insight into the impact of RNA decay to changes in total RNA abundance following inhibition of the general transcription machinery and associated factors in cancer.

RESULTS

Transcriptional inhibition selectively reduces total mRNA levels

To assess whether the therapeutic response to transcriptional inhibition is selective, SLAM-seq was performed on K562 cells treated with small molecule inhibitors of p300/CBP (A-485), BRD4 (JQ1), CDK9 (AZ-5576) and RNAPII (ACTD) [26] (Fig. 1A, B). The on-target activity of p300/CBPi, BRD4i and CDK9i was validated by western blot analysis of H3K18ac, c-MYC protein and RNAPII carboxy-terminal domain (CTD) Serine 2 (Ser2) phosphorylation, respectively [14,33,34] (Fig. S1. A). Differential gene expression analysis (DGEA) of total messenger RNA (mRNA) read counts from SLAM-seq libraries normalized to an external spike-in of *Drosophila melanogaster* Schneider 2 (S2) cell RNA revealed that all transcriptional inhibitors affected the levels of only a fraction of expressed genes (Fig. 1C, D). Principal component analysis (PCA) of total mRNA changes highlighted distinct responses to p300/CBPi, BRD4i, CDK9i and ACTD, whereby CDK9i and ACTD signatures co-clustered and exhibited the highest degree of similarity (Fig. S1. B). Consistent with previous studies [20,35], 785 SEs defined using publicly available H3K27ac ChIP-seq data in K562 cells (Fig. 1E) and 83 CR SE-associated TFs identified using the Coltron algorithm (Fig. 1F, G) were significantly more down-regulated compared to all other genes (Fig. 1H, I). Moreover, Gene Set Enrichment Analysis (GSEA) highlighted negative enrichment of several cancer and inflammatory hallmark pathways, including MYC targets and cytokine signalling, respectively (Fig. 1J). However, the vast majority of genes were refractory to changes in total mRNA levels at these timepoints and inhibitor concentrations (Fig. 1C, D), including several SE associated genes and CR TFs (Fig. S1. C, D).

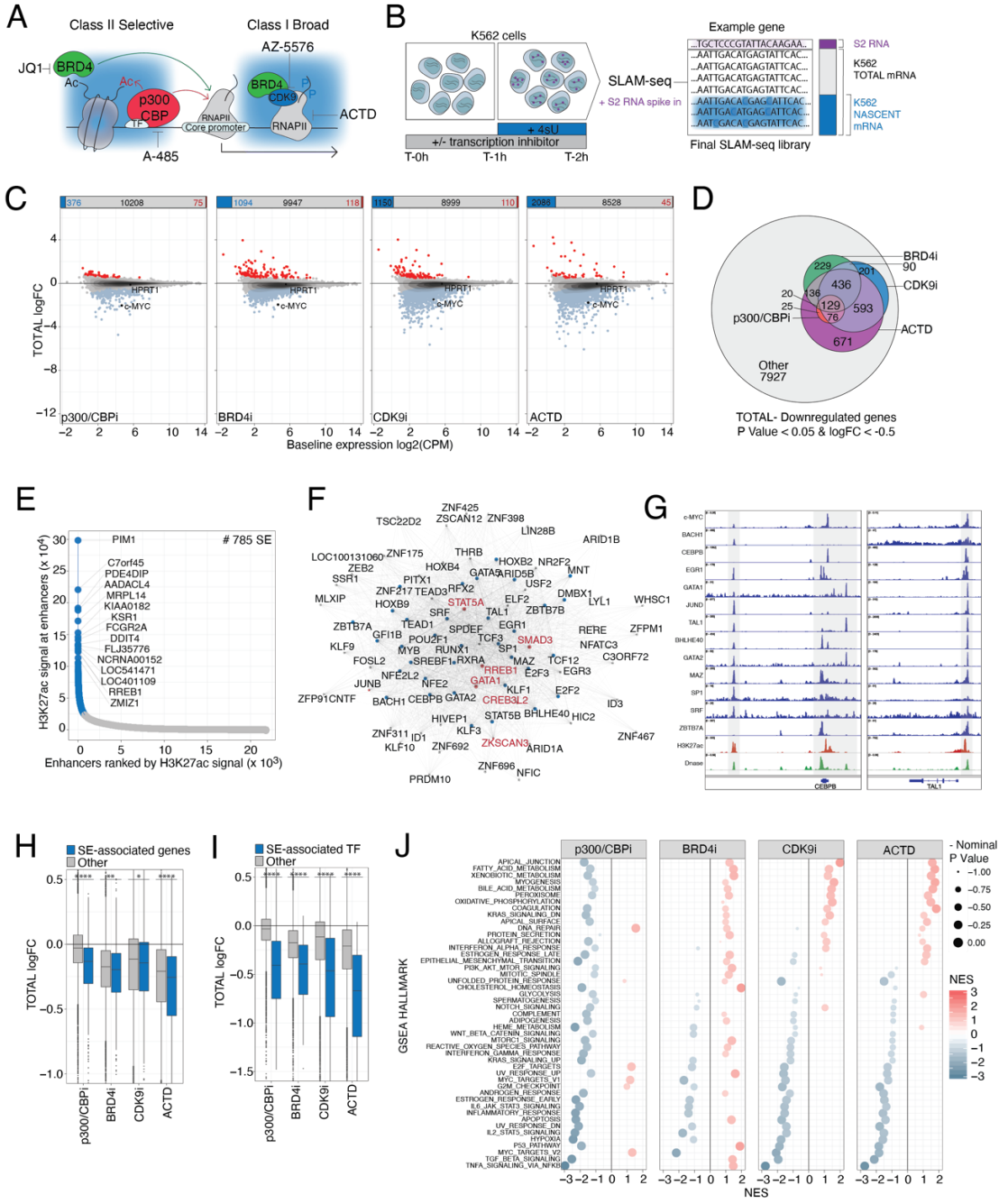

Figure 1 Transcriptional inhibition results in selective changes in total RNA levels

(A) Simplified schematic of transcription inhibition by A-485 (p300/CBPi), JQ1 (BRD4i), AZ-5576 (CDK9i) and Actinomycin D (ACTD). **(B)** Schematic of SLAM-seq experimental procedure. Nascent reads are defined as RNA containing at least two thymine-to-cytosine (T>C) conversions and total reads are defined as the sum of unconverted and converted RNA. Schneider 2 (S2) RNA was spiked-in as an external reference control. **(C)** Scatterplot of baseline total mRNA expression versus change in spike-in normalized total expression upon two hours of transcription inhibition. Significantly up- or down-regulated genes highlighted in red and blue, respectively. Sum of significantly differentially altered events indicated in bar chart above. **(D)** Venn diagram of significantly down-regulated genes for each treatment condition using spike in normalized total mRNA reads. Remaining genes indicated as 'other.' **(E)** Super-enhancer (SEs; blue) and enhancers (grey) ranked by H3K27ac signal. A total of 785 SEs were identified and genes associated with the top 15 are highlighted. **(F)** Network plot of SE-associated core-regulatory (CR) transcription factors (TFs) identified using the Coltron algorithm [35]. TFs previously identified as part of K562 cell core regulatory networks highlighted in red [34]. **(G)** Integrated Genomics Viewer (IGV) screen shots of *CEBPB* and *TAL1* genomic loci with CR TF occupancy obtained from ENCODE. **(H)** Boxplot of spike-in normalized total gene expression of SE-associated genes or **(I)** SE-associated CR TFs relative to all other genes upon two hours of transcription inhibition. (J) Gene Set

Enrichment Analysis (GSEA) Normalized Enrichment Scores (NES) and significance of cancer hallmark pathways using ranked total mRNA changes upon two hours of transcription inhibition.
RNAPII: RNA Polymerase II. TF: Transcription factor. BRD4: Bromodomain-Containing Protein 4. p300/CBP: p300/cAMP-response element binding protein (CBP). CDK9: Cyclin Dependent Kinase 9. Ac: Acetyl group. P: Phosphate group. 4sU: 4-thiouridine. H: Hour. 3'UTR: 3' Untranslated Region. LogFC: log2 fold change relative to DMSO. Baseline expression: spike-in normalized total log2 CPM in DMSO-treated conditions. CPM: Counts Per Million. Significantly up-regulated: P Value < 0.05 & logFC > 0.5. Significantly down-regulated: P Value < 0.05 & logFC < -0.5. ****, **, *: P Value < 0.0001, < 0.01 and <0.05, respectively, using an unpaired Wilcoxon test.

Transcriptional inhibition broadly perturbs nascent RNA production

To investigate whether selective changes in total mRNA levels following small molecule inhibition of p300/CBP, BRD4, CDK9 and RNAPII are due to a concordant change in mRNA production, DGEA was performed on spike-in normalized nascent read counts as marked by at least two T > C conversions in 3'UTR derived reads (Fig. 1B). In contrast to the effect seen on total mRNA (Fig. 1C, D), nascent mRNA was more broadly repressed in response to all inhibitors (Fig. 2A, B, S1. E). The greatest effect on nascent mRNA expression was observed following treatment with CDK9i and ACTD, and due to their ability to globally down-regulate the *de novo* mRNA synthesis of > 80% of genes, these agents were termed broad or class I inhibitors (Fig. 1A, 2A, B). In contrast, transcriptional inhibition with p300/CBPi and BRD4i, designated henceforth as class II compounds, was selective and significantly reduced the mRNA synthesis of < 50% of expressed genes (Fig. 1A, 2A, B). Importantly, changes in nascent gene expression with class II inhibitor treatment was still significantly greater in comparison to associated total mRNA changes (Fig. S2. F). In agreement with differences observed between total and nascent mRNA levels seen following treatment with all transcriptional inhibitors tested (Fig. S2. F), comparison between these two modalities revealed only a modest Pearson's correlation coefficient (Fig. 2C). Correlations were lower with class I inhibitors (0.17-0.3) in comparison to more selective transcriptional perturbation with class II compounds (0.43-0.46) (Fig. 2C). As an example of the disconnect between changes in nascent and total mRNA abundance, genes such as *HPRT1* that were the least responsive (P-value > 0.05, -0.25 < logFC < 0.25; 200 genes closest to the mean logFC) to changes in total mRNA had significantly down-regulated nascent gene expression, especially in response to class I compounds (Fig. 2D, E). In contrast, the proto-oncogene *c-MYC* was amongst the most responsive to transcriptional perturbation (top 200 genes most significantly down-regulated) on both total and nascent mRNA levels (Fig. 2D, F). This highlights that in a subset of genes, down-regulation of *de novo* mRNA synthesis can result in a concomitant reduction in total mRNA. However, despite global down-regulation of nascent transcripts, most genes appear to be refractory to changes in total mRNA following acute transcriptional inhibition. Taken together, these data suggest that post-transcriptional gene-intrinsic parameters that define total mRNA levels might be driving down-regulation of a discrete subset of genes upon transcriptional perturbation.

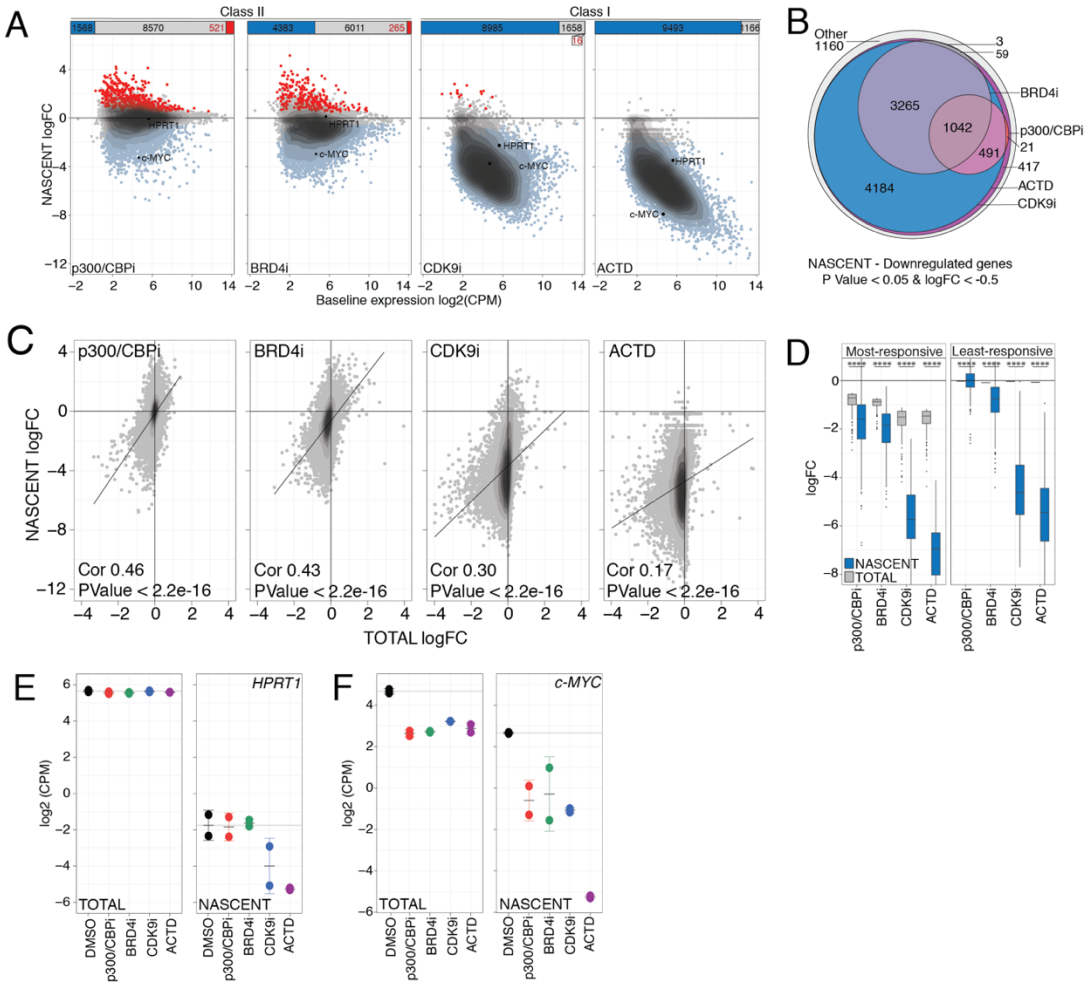

Figure 2 Nascent and total mRNA changes are disconnected upon transcriptional perturbation
(A) Scatterplot of baseline total mRNA expression versus change in spike-in normalized nascent expression upon two hours of transcription inhibition. Significantly up- or down-regulated genes highlighted in red and blue, respectively. Sum of significantly differentially altered events indicated in bar chart above. **(B)** Venn diagram of significantly down-regulated genes for each treatment condition using spike in normalized nascent mRNA reads. Remaining genes indicated as 'other.' **(C)** Scatter plot of spike-in normalized total and nascent gene expression upon two hours of transcription inhibition. **(D)** Change in spike-in normalized total and nascent expression of **(*left*)** most- and **(*right*)** least-responsive genes. **(E)** Spike-in normalized **(*left*)** total and **(*right*)** nascent mRNA expression of *HPRT1* or **(F)** *c-MYC* upon two hours of transcription inhibition.
Baseline expression: spike-in normalized total log2 CPM in DMSO-treated conditions. CPM: Counts Per Million. Significantly up-regulated: P Value < 0.05 & logFC > 0.5. Significantly down-regulated: P Value < 0.05 & logFC < -0.5. Cor: Pearson's correlation co-efficient. ****: P Value < 0.0001 using an unpaired Wilcoxon test.

Core Regulatory Transcription Factors are encoded by highly produced and labile transcripts
mRNA decay rates determine total transcript levels [36]. To investigate whether mRNA stability influences changes in total mRNA levels following transcriptional inhibition, we first directly measured mRNA half-lives in K562 cells using 4sU pulse-chase combined with SLAM-seq [26] (Fig. 3A, S2. A). Decay kinetics were quantitatively determined by fitting exponential decay functions to normalized transcript levels measured over the time-course and estimating the mRNA half-lives ($t_{1/2}$) (Fig. 3A). As cellular division results in the dilution of 4sU derived reads, half-life measurements were further normalized to the cell cycle (Fig. S2. B), generating estimated decay parameters for 6580 genes (Fig. 3B), including for short-lived genes such as *c-MYC* ($t_{1/2}$ = 1.3 hours) (Fig. 3C), which were concordant with published decay measurements obtained in K562 cells with conversion-based protocols (Fig. S2. C) [28,37]

To assess whether gene function is indeed related to mRNA half-life, transcript decay measurements were divided into pentiles and the most short- and long-lived groups were used for gene ontology (GO) analysis (Fig. 3D). Genes with the shortest half-lives were enriched for those encoding TFs and transcription regulators (Fig. 3D). In contrast, long-lived transcripts were over-represented for terms related to cellular homeostasis and metabolism (Fig. 3D). As *de novo* mRNA synthesis also determines total transcript abundance [36], it was determined whether mRNA production in addition to decay is correlated with gene function. Production rates for each gene were first obtained by subjecting K562 cells to 4sU labelling for 5 and 15 minutes, followed by transient transcriptome (TT) -seq, after which 4sU-containing nascent RNA was isolated via affinity purification and sequenced [29]. mRNA synthesis measurements were then divided into pentiles and compared to decay groups previously defined. Despite GO term analysis demonstrating that genes with the shortest half-life and either very high (pentile 5) or low (pentile 1) production rates both encoded for TFs (Fig 3D), only those with high mRNA synthesis rates were enriched for CR TFs (Fig. 1F. G, 3D, S2. D). These findings suggest that in order to rapidly and accurately control their expression, transcripts encoding key lineage specific and CR TFs may have evolved to be extremely labile, resulting in rapid decay and necessitating high productions rates in order to maintain cellular mRNA levels. As such, the frequently observed association between CR TFs and genomic elements such as super-enhancers to drive high-level expression may be driven by the continual need to synthesize *de novo* RNA due to their short intrinsic half-lives [1,38]. Conversely, long lived mRNA with low production kinetics were related to exocytic and organelle fusion processes, and those with high synthesis rates with cellular translation and metabolism (Fig 3D). This highlights that slow mRNA dynamics are critical for roles that ensure constant and normal cellular homeostasis.

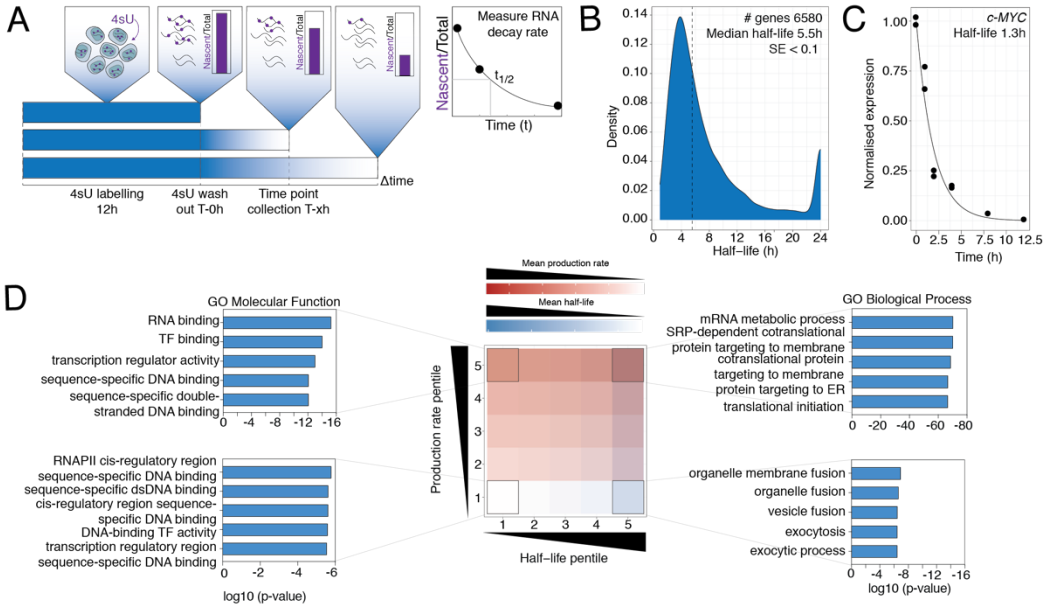

Figure 3 RNA decay is strongly related to gene function
A) Schematic of 4-thiouridine (4sU) pulse labelling and chase. T > C conversion rates were calculated for each time point, normalized to 0-h and fit with exponential decay functions derive half-life ($t_{1/2}$). **(B)** Distribution of mRNA stability of 6580 genes in the K562 cell line. **(C)** *c-MYC* transcript half-life estimation. Half-life values represented are from technical duplicates and normalized for K562 cell division time from S2. B. **(D)** Heatmap of mean mRNA half-life (blue) and production rate (red) for each mRNA decay and production pentile. Gene Ontology (GO) terms of genes within subsets highlighted in black are indicated in bar charts.
H: hour. SE: Standard Error.

Gene-intrinsic RNA decay properties shape the response to transcriptional inhibitors

The vast majority of publications studying the effect of transcriptional/epigenetic compounds in cancer share the observation that selective gene expression responses arise from perturbation of core RNAPII machinery. The selectivity is generally attributed to gene-specific chromatin features, including occupancy of the targeted factor, cell-type specific TFs and super-enhancers [1,32], all of which impact the *de novo* production of RNA. In the context of cancer this has been described to primarily affect oncogenic networks driven by key TFs such as *c-MYC* [32,39–41]. In light of our observation that transcripts within these oncogenic networks are rapidly turned over through a cycle of rapid production and decay (Fig. 3), we hypothesized that gene-intrinsic parameters are the causative factor driving selective total transcriptional changes to perturbation of the core-transcriptional machinery. Indeed, the most responsive genes to class I and II inhibitors (Fig. 2D) were approximately 3-4 times more shorter-lived than those least responsive to RNAPII-targeting, and the median half-life of each category varied little between class I- or II- mediated transcriptional inhibition (Fig. 4A). Conversely, previously defined mRNA decay pentiles (Fig. 3D) revealed that the 20% most short-lived genes were significantly down-regulated in comparison to longer-lived gene groups on the total mRNA level with all compounds tested (Fig. S2. E), and were enriched for genes defined as the most responsive (Fig. 4B). This was more evident with class I compounds, where >90% of most responsive genes were in the shortest $t_{1/2}$ group (Fig. 4B). Contrarily, genes that were least responsive to RNAPII-targeting were over-represented for longer $t_{1/2}$ gene categories (Fig. S2. F), indicating that transcripts with slow decay kinetics maintained total mRNA levels following acute transcriptional inhibition. In addition, mRNA production rates were predictive of total mRNA downregulation only in the context of transcript half-lives, where genes with the highest mRNA production rates (pentile 5; 4.2e-02- 6.7 FPKMh^{-1}) and shortest half-lives (pentile 1; $t_{1/2}$0.9-3.3 hours) were most strongly repressed (Fig. 4C). Moreover, the most-responsive genes (Fig. 2D) were enriched (25.5-37%) in the shortest lived and most highly produced subset (Fig. 4C), where this was not observed for genes least-responsive (Fig. 2D, S2. G).

To quantitatively assess the impact of transcript half-lives to total mRNA abundance upon transcriptional inhibition *in silico*, we developed a mono-exponential model of steady state gene expression using only mRNA production and decay rates (Fig. 4D). Production rates (k_1) and decay rates (k_2) were determined as described above. Predicted steady state mRNA levels obtained using the ratio of synthesis and decay rates for each gene significantly correlated with experimental measurements of baseline mRNA abundance (Pearson's correlation coefficient 0.65) (Fig. S2. H), indicating that the model was sufficiently accurate to estimate equilibrium mRNA levels with a variety of initial conditions and time intervals.

To investigate *in silico* the effect of mRNA decay on total transcript levels upon complete abrogation of *de novo* mRNA synthesis, the production rate of each gene was set to zero and total mRNA abundance was modelled after two hours (Fig. 4D, S2. I). Consistent with experimental data (Fig. 2E, F), *c-MYC* and *HPRT1* were found to be down-regulated with logFC values of -1.53 and -0.06, respectively (Fig. S2. I). Functional annotation of genes down-regulated in this model of transcriptional shutdown using GSEA revealed significant negative enrichment of cytokine signalling, inflammatory and *c-MYC* target cancer hallmark pathways and SE-transcriptional programs (Fig. 4E). Moreover, additional gene ontology (GO) analysis using ToppGene [42–44] of the top 200 most down-regulated genes, which

included oncogenes such as *c-MYC* (Fig. S2. J), demonstrated signatures associated with TF function [45] (Fig. 4F).

Correlation analysis between *in silico* and experimental total mRNA measurements of transcriptional perturbation revealed that class I inhibitors resulted in gene expression changes that were significant and highly similar to a modelled complete abrogation of nascent transcription (Pearson's correlation coefficient 0.59-63) (Fig. 4G). Conversely, changes in total mRNA levels following treatment with class II compounds only modestly correlated with the model (Pearson's correlation coefficient 0.26-0.34) (Fig. 4G). In agreement with these results, receiver operator characteristic (ROC) analysis and derivation of the area under the curve (AUC) of simulated and experimental total mRNA levels revealed that genes with short RNA $t_{1/2}$ were strongly predicted to be more responsive to RNAPII targeting (Fig. 4H). Predictive accuracy was higher with class I inhibitors (AUC 0.93-0.94) in comparison to class II (AUC 0.86-0.90) (Fig. 4H). This firstly highlights that any change in total mRNA levels following global perturbation of mRNA production with class I inhibitors is strongly determined by mRNA half-lives. Secondly, these data also suggest that changes in total mRNA levels of distinct genes mediated by class II compounds stems from a combination of selective inhibition of *de novo* mRNA synthesis and gene intrinsic RNA $t_{1/2}$.

Analysis of an independent SLAM-seq data from K562 cells (Fig. S3A-D) revealed transcript half-life also defines the response to transcriptional disruption through small molecule mediated inhibition of BRD4 or CDK9, as well as, acute protein degradation of MYC and BRD4 (Fig. S3E-I). In addition, short-lived transcripts were most sensitive to inhibition of BCR-ABL1 signalling (Fig. S3E-I). Concordant with our observations, the magnitude of nascent RNA responses greatly exceeded those on the total RNA level, indicating that transcript stability greatly buffers this response, which has therapeutic implications. To extend our findings to another cell line we measured RNA decay parameters (Fig. S4A, B) and transcriptional responses to therapeutically relevant (Fig. S4C, D) compounds in THP-1 cells. This revealed that similar to K562 cells, that the total mRNA response in this THP-1 cells to a distinct BET, CDK9, CDK12/13 and CDK7 inhibitors was largely dependent on gene-intrinsic decay properties, with a much larger transcriptional response observed on the nascent RNA level (Fig. S4E-H).

Reciprocal adjustments in RNA synthesis and decay rates to maintain total cellular RNA concentrations is a phenomenon called 'transcriptional buffering' [47]. To determine if therapeutic perturbation of RNAPII transcription affected RNA decay rates via transcriptional buffering, RNA half-lives were measured using 4sU pulse-chase combined with SLAM-seq in the presence of either JQ1 (BRD4i, class II) or AZ-5576 (CDK9i, class I) (Fig. S5A). This demonstrated that BETi modestly increased RNA decay rates, and resulted in a lower mean half-life of 4.92 hours (Fig. S5B, C). In contrast, CDK9i treatment broadly decreased RNA rates, increasing the mean RNA half-life in K562 cells to 6.62 hours (Fig. S5B, C). This observation is consistent with prior reports demonstrating that loss of core RNAPII machinery, such as RNAPII, the pre-initiation complex (PIC) and Mediator, increases RNA half-lives [47]. Importantly, modelling of complete transcriptional shutdown using treatment specific RNA decay rates (Fig. S5D) correlated significantly with experimentally measured total RNA changes (Fig. S5E), indicating that transcriptional buffering does not negate the importance of RNA decay rates in shaping the total mRNA response to the class of therapeutic transcriptional inhibitors.

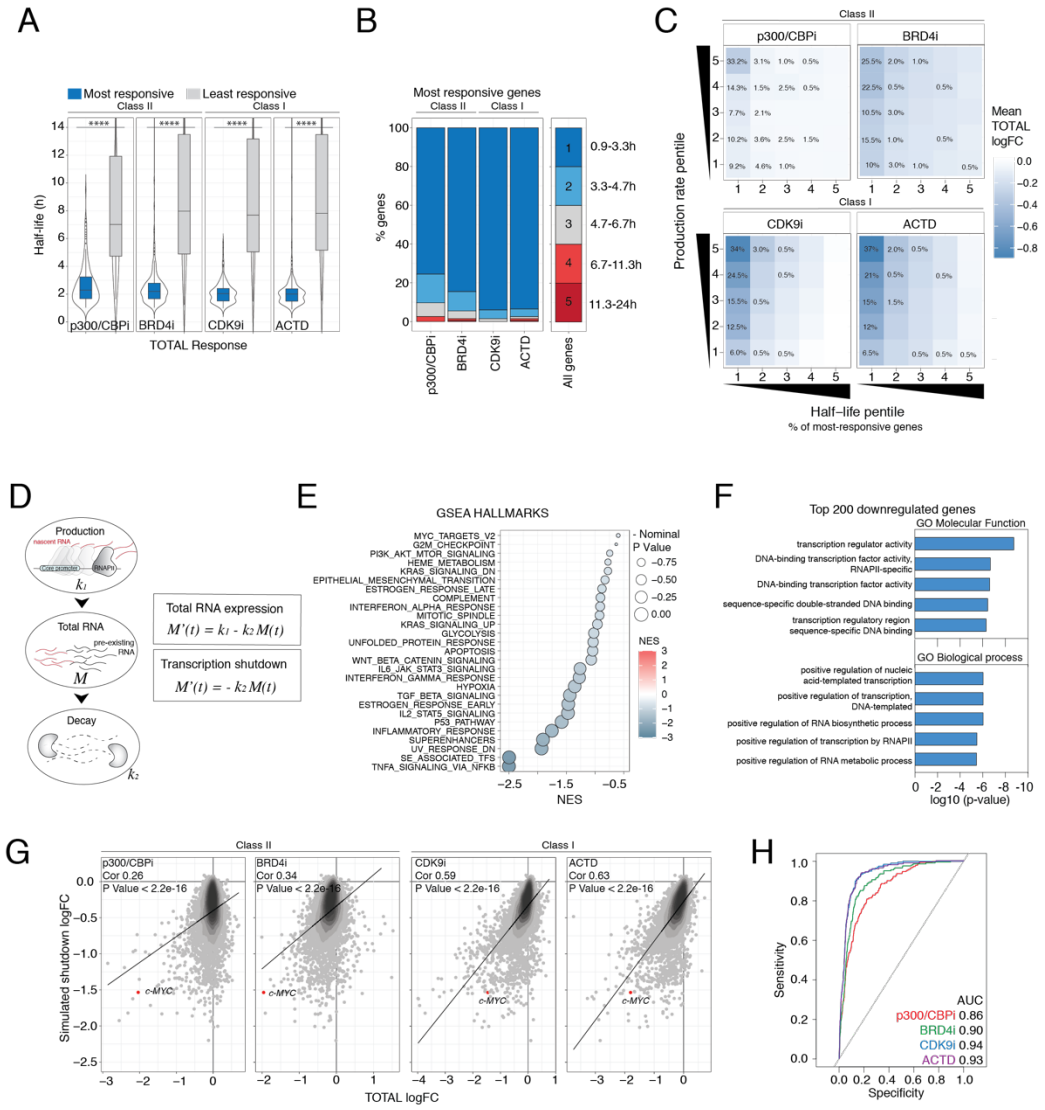

Figure 4 RNA decay is a critical determinant of gene sensitivities to transcriptional inhibition

(A) Boxplot of mRNA half-lives of genes most- and least-responsive to treatments indicated. **(B)** Stacked bar chart of mRNA half-life pentiles in genes most-responsive to treatments indicated. **(C)** Heatmap of mean total mRNA logFC for each mRNA decay and production pentile. Numbers indicated are percentage of most-responsive genes within each subset. **(D)** Mathematical model of mRNA production (k_1) and decay (k_2). ***(Top right)*** Differential equation describing total mRNA. ***(Bottom right)*** Simulation of total mRNA levels with complete transcription shutdown. **(E)** GSEA analysis of hallmark, SE and SE-associated TF gene sets using simulated total gene expression following complete transcription shut-down ranked by z-scored logFC values. Signatures with Normalized Enrichment Scores (NES) < 0 shown. **(F)** GO analysis of the top 200 most down-regulated genes with simulated total transcription shutdown for two hours indicated in blue in S2. J. **(G)** Scatter plot of simulated total gene expression response following two hours of complete transcription shutdown and measured total gene expression response to inhibitors indicated. **(H)** Receiver Operator Characteristic (ROC) analysis of total logFC with treatments indicated and simulated total logFC after complete transcription shutdown for 2 hours. logFC values were binarized according to whether genes were most-responsive to treatments indicated.

****: P Value < 0.0001, using an unpaired Wilcoxon test. Most-responsive: top 200 most significantly down-regulated genes (logFC < -0.5 and P Value < 0.05) using spike-in normalized total reads. Least-responsive: 200 unaltered (-0.25 < logFC < 0.25 and P Value > 0.05) genes using spike-in normalized total reads. logFC: log2 fold change relative to DMSO or 0 hours. AUC: Area Under the Curve.

Despite these analyses being completely agnostic to the chromatin landscape or the molecular consequences of the core-transcriptional component targeted, they were able to effectively isolate a group of responsive genes to all forms of transcriptional perturbation. This highlights that the selectivity of these therapies is over-estimated

and suggests that oncogenic and pro-inflammatory networks driven by short-lived and highly produced TFs are intrinsically sensitized to any form of abrogation of *de novo* RNA synthesis, thus challenging the notion that selective targeting is required to specifically disrupt oncogenic transcription. Finally, particular genomic elements, such as SEs, may correlate with transcriptional responses to this class

MAC-seq defines the role of RNA decay to changes in gene expression with 73 transcriptional and epigenetic compounds

To assess the role of mRNA half-life to gene expression responses across a wider range of clinically relevant inhibitors, we used Multiplexed Analysis of Cells sequencing (MAC-seq) to profile changes in total mRNA levels in response to 73 small molecule inhibitors of epigenetic and transcriptional proteins in K562 cells, where previously tested drugs (Fig. 1-4) were included as controls [48] (Fig. 5A, S6. A). De-multiplexing of treatment conditions and DGEA thereafter revealed a number of differentially expressed events (Fig. 5B), where only eight out the 73 compounds tested globally repressed transcription and significantly down-regulated > 1000 genes (Fig. 5C). This first class of inhibitors (class I) consisted of those able target t-CDKs and the core RNAPII machinery (Pan-Tx) (Fig. 5C, S6. A). Moreover, a second group (class II) of an additional six drugs targeting BRD4, p300/CBP, pan-histone deacetylases (HDACs), and protein phosphatases (PP), were able to selectively down-regulate a subset of least 200 genes (Fig. 5C, S6. A). Despite technical and experimental differences between the MAC- and SLAM-seq protocols, analysis of MAC-seq total mRNA abundance relative to the External RNA Control Consortium (ERCC) RNA external reference control, recapitulated the segregation of the tested compounds into class I and II (Fig. 2A, Fig, 5C). Remaining compounds, defined as class III, that targeted histone demethylases (HDMe) and methyltransferases (HMe), DNA alkyl- (DNA AGT) and methyl-transferases (DNAMe), sirituin (SIRT), PARP, HuR/ELAVL1 and topoisomerases (Topo) either repressed the expression of a minimal number of genes (< 200) or primarily up-regulated transcription (% down- or up- regulated < 50%) (Fig. 5C). This indicates that gene-intrinsic RNA stability most likely has minimal influence on the total transcriptome for class III compounds.

Uniform Manifold Approximation and Projection (UMAP) of drug treatments revealed that gene changes grouped according to drug treatment (Fig. S6. B, *middle*), drug protein target (Fig. S6. B, *bottom*) and family (Fig. 5D, *top*) and class (Fig. 5D, *middle*). Notably, despite all class I compounds forming an entirely distinct cluster (Fig. 5D, *middle*), more detailed PCA analysis of this drug class in an isolated setting revealed separation between Pan-Tx, CDK9/7/12/13 and CDK11/12/13 inhibitors (Fig. 5D *bottom*, S6. A). This suggests that though class I compounds are able to broadly repress gene expression, they are mechanistically distinct and not equivalent. Inhibitors within the class II category however, with the exception of drugs targeting BET proteins, clustered separately (Fig. 5D *bottom*, S6. A), highlighting that they induce distinct and selective transcriptional responses.

Data from figures 1-4 demonstrated that RNA decay is a critical determinant to changes in total gene expression following transcription inhibition with p300/CBPi, BRD4i, CDK9i and ACTD, so it was determined if these findings could be extended to other compounds able to globally (class I) or selectively (class II) repress gene expression as defined by MAC-seq (Fig. 5C). Genes most responsive (top 200 genes most significantly down-regulated) to class I and II inhibitors were significantly shorter lived in comparison to genes least responsive (P-Value > 0.05, -0.25 < logFC < 0.25; 200 genes closest to the mean logFC) to transcriptional targeting (Fig. 5E, S6. C).

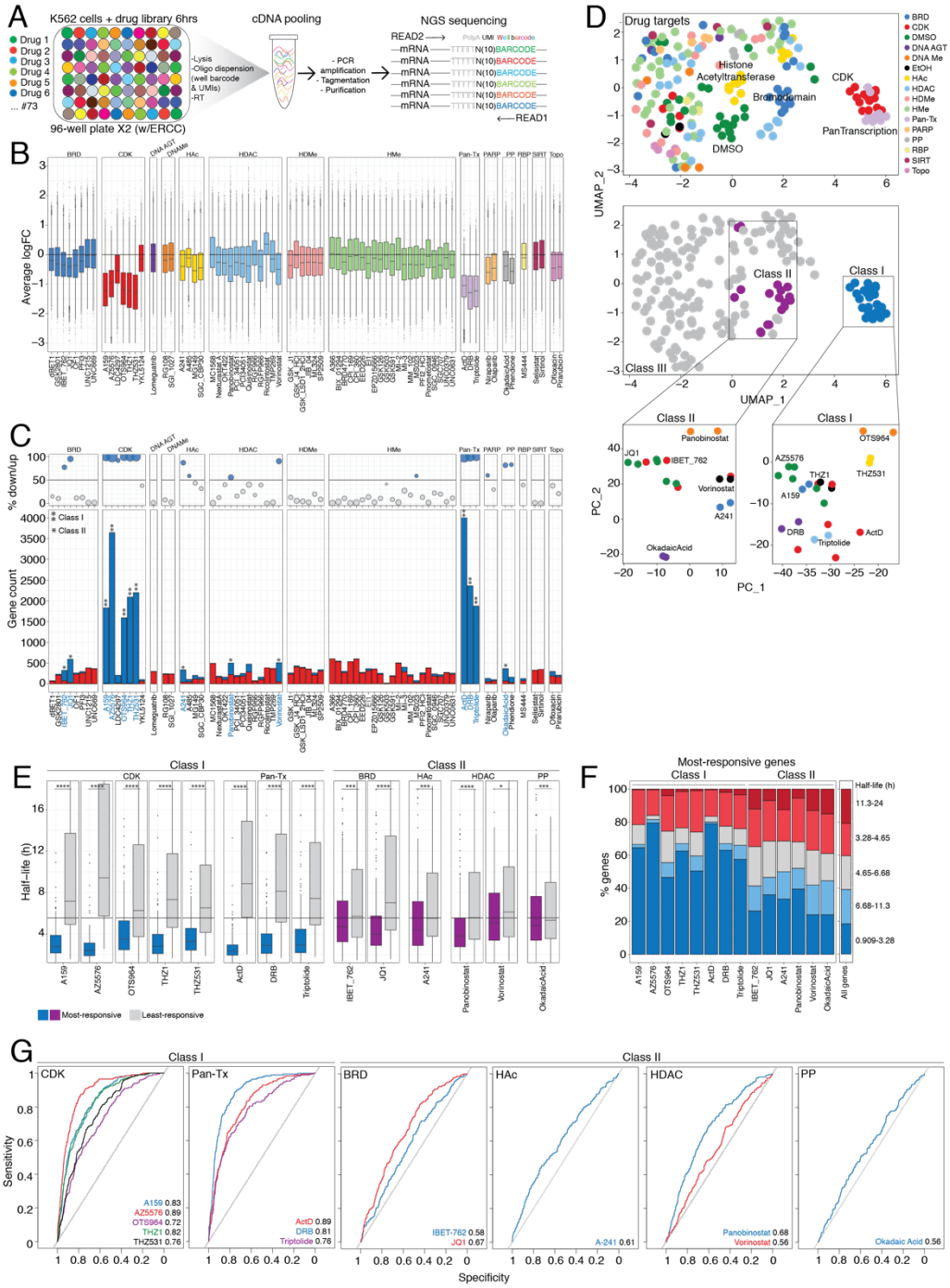

Figure 5 RNA half-life strongly shapes transcriptional response to transcriptional and epigenetic inhibitors as defined by MAC-seq

(A) Schematic of MAC-seq experimental procedure. **(B)** Box plot of change in gene expression relative to DMSO/EtOH controls with inhibitors indicated. Inhibitors are grouped according to drug protein target family. **(C)** (***Top***) Percentage ratio or (***bottom***) absolute number of significantly up- and down-regulated genes. Inhibitors able to significantly down-regulate > 1000 genes are termed 'Class I' and by **. Inhibitors able to significantly down-regulate > 200 genes are termed 'Class II' and indicated by *. Remaining compounds as designated as class III. **(D)** Uniform Manifold Approximation and Projection (UMAP) of treatment conditions with (***top***) drug protein target family (***middle***) or pre-defined classes highlighted. (***Bottom***) PCA plot of drug classes **(right)** II and **(left)** I with drug names shown. **(E)** Boxplot of mRNA half-life of most- and least-responsive genes to class I and II inhibitors. **(F)** Bar chart representation of mRNA half-life pentiles in genes most-responsive to class I and II inhibitors. **(G)** Receiver Operator Characteristic (ROC) analysis of logFC with class I and II inhibitors and simulated total logFC after complete

transcription shutdown for 6 hours. logFC values were binarized according to whether genes were most-responsive to treatments indicated.
UMI: Unique Molecular Identifier. logFC: log2 fold change. BRD: Bromodomain. CDK: Cyclin Dependant Kinase. DNA AGT: DNA alkyl-transferase. DNAMe: DNA methyl-transferase. HAc: Histone acetylase. HDAC: Histone deacetylase. HDMe: Histone demethylase. HMe: Histone methyl-transferase. Pan-Tx: Pan-transcription. PP: Protein Phosphotase. RBP: RNA Binding Protein. SIRT: Sirtuin. Topo: Topoisomerase. Significantly up-regulated: P-Value < 0.05 and average logFC > 0.5. Significantly down-regulated: P-Value < 0.05 and average logFC < -0.5. logFC: log2 fold change relative to DMSO/EtOH. AUC: Area Under the Curve. Most-responsive: top 200 most significantly down-regulated genes (logFC < -0.5 and P Value < 0.05) using spike-in normalized reads. Least-responsive: 200 unaltered (-0.25 < logFC < 0.25 and P Value > 0.05) genes using spike-in normalized reads.

The difference in half-life between most and least responsive gene sets was most striking with class I inhibitors, where mRNA stability varied up to three-fold between the two categories (Fig. 5E, S6. C). Consistently, the 20% most short-lived genes, as defined previously in Fig. 3, were enriched as genes most responsive to transcriptional targeting by class I and II inhibitors (Fig. 5F). This was more evident with class I compounds, which had > 40% of most-responsive genes within the most short-lived pentile (Fig. 5F). In agreement with these data, AUCell analysis revealed that the same half-life pentile was significantly depleted within the top 10% most highly abundant genes that responded to class I compounds in comparison to class II and III (Fig. S6. E). The 20% most long-lived genes were under-represented as genes most-responsive to class I- and II-type transcriptional perturbation, but more enriched in genes least-responsive to targeting by most inhibitors within the two classes (Fig. S6. D). Genes with the longest half-lives were also found to be significantly enriched within highly expressed genes in response to class I and II compounds compared to class III (Fig. S6. F). Furthermore, ROC analysis and derivation of the AUC of simulated total mRNA levels following complete abrogation of *de novo* transcription and gene expression changes to class I and II inhibitors (Fig. 5B) revealed that genes with short half-lives were highly predictive as genes amenable to t-CDK and general RNAPII inhibition (Fig. 5G), consistent with previous findings (Fig. 4H). Due to selective targeting observed on the nascent mRNA level and longer drug incubation times, predictive accuracy was modest with BRD4, p300/CBP, pan-HDAC and PP targeting (Fig. 5G). Taken together, these data demonstrate that the role of mRNA decay can be extended to several transcriptional and epigenetic inhibitors, where both selective and global down-regulation of gene expression is strongly dictated by gene intrinsic properties including RNA stability.

c-MYC RNA stabilization is sufficient to confer resistance to transcriptional targeting

Sequence motifs within the 3' UTR of genes strongly influence the decay rate of eukaryotic transcripts [49,50]. For example, inflammatory and immune mediators, and oncogenes including *TNF*, *PD-L1* and *c-MYC*, have unstable mRNAs implicated with the presence of AU-rich elements (AREs), AUUUA and miRNA recognition motifs within their 3'UTR [51–55].

To functionally investigate whether gene-intrinsic RNA decay properties are the key determinant in shaping the response to transcriptional inhibition, we decided to alter the RNA decay parameters of the *c-MYC* oncogene via its 3'UTR, whilst preserving the endogenous chromatin context. Using CRISPR/Cas9 -mediated homology directed repair (HDR) in K562 cells, the *c-MYC* endogenous 3'UTR was substituted with the 3'UTR of the longer-lived gene *HPRT1* with a destabilized GFP (dsGFP) reporter, termed '*c-MYC-HPRT1* 3'UTR' (Fig. 6A). Designated as '*c-MYC*-control 3'UTR', dsGFP was knocked-in 5' of the endogenous *c-MYC* 3'UTR sequence as a control cell line (Fig. 6A). Validation of HDR was assessed with PCR using primers amplifying regions around and within the *c-MYC* 3'UTR

genomic locus (Fig. S7. A-F), where PCR fragments were of lengths corresponding to successful knock-in of either *dsGFP* only (S4. A-D) or *dsGDP* and *HPRT1* 3'UTR sequences (S7. A, B, E, F). Sanger sequencing of the same PCR fragments revealed 100% homology between products and defined *P2A*, *dsGFP* and/or *HPRT1*-3'UTR sequences (S7. G, H).

RNA stability for *c-MYC* was assessed using quantitative real time (qRT) -PCR, which demonstrated that knock-in of the *HPRT1* 3'UTR increased the half-life of the chimeric *c-MYC* transcript by approximately eight hours in response to ActD, representing a four-fold increase over the half-life of the endogenous and entopic *c-MYC* transcripts (Fig. 6B, S8. A, B). Interestingly, *c-MYC* mRNA in the *c-MYC-HPRT1*-3'UTR cell line was not as stable as endogenous *HPRT1* transcripts, suggesting that *c-MYC* mRNA stability is influenced not only by its 3'UTR (Fig 6B, S8. A, B). This is consistent with previous studies demonstrating that important decay elements are located in the third exon of the coding sequence of *c-MYC* [53].

As mRNA production and decay may both determine total mRNA levels, we investigated whether increased *c-MYC* transcript stability influenced its nascent and total mRNA abundance. Whole transcriptome RNA-seq followed by DGEA of exon read counts in DMSO-treated conditions revealed that steady state total *c-MYC* mRNA expression between *c-MYC*-control and *-HPRT1* 3'UTR cell lines was unaltered (Fig. 5C, S8. C). Moreover, *c-MYC* nascent mRNA abundance, inferred using intron read counts, was significantly lower in the c-*MYC-HPRT1* 3'UTR cell line in comparison to *c-MYC*-control 3'UTR (Fig. S8. D). This was not completely unexpected as mRNA synthesis and degradation are linked processes, and alteration of either has been demonstrated to result in a phenomenon called 'transcript buffering' [56].

Gene sensitivities to transcriptional perturbation have largely been associated SEs and CR TFs [21,57]. As our system genetically engineered the endogenous 3'UTR of *c-MYC*, its genomic location, in addition to *cis*- and *trans*-factors that impact its regulation remained unaffected. This therefore enables the direct assessment of altered mRNA stability to transcription targeting within the wild type chromatin context. To investigate the response of stabilized *c-MYC* to RNAPII targeting, c-*MYC*-control and *-HPRT1* 3'UTR cell lines were treated with the class I compounds AZ-5576 (CDK9i) or ACTD for six hours, and whole transcriptome RNA-seq was performed. Consistent with previous findings (Fig. 1, 2, 5), DGEA analysis of exon and intron external spike-in normalized reads revealed a global decrease in total and nascent gene expression, respectively (Fig. S8. E-G).

To determine whether altered *c-MYC* mRNA stability influenced nascent responses to CDK9i and ACTD treatment, we compared *c-MYC* intronic counts between c-*MYC*-control and *-HPRT1* 3'UTR cell lines following transcription perturbation. D*e novo* *c-MYC* synthesis was significantly down-regulated with each compound irrespective of mRNA half-life (Fig. 5C *right*). In contrast, assessment of *c-MYC-dsGFP* total RNA (Fig. 5C *left)* and protein abundance (Fig. 5D-G, S8. H) revealed that *c-MYC* stabilization rendered it less sensitive to targeting by either compound. The resistance to RNAPII targeting on the total mRNA level was *c-MYC* specific, as *c-MYC* was the most significantly altered gene with each treatment (Fig. 5H) and PCA of spike-in normalized total mRNA changes highlighted that conditions clustered according to inhibitor and not cell line (Fig. S8. I). Consistently, correlation analysis of all DEGs in c-*MYC*-control and *-HPRT1* 3'UTR cell lines with CDK9i and ACTD revealed that changes were highly similar and statistically significant (Pearson's correlation coefficient 0.96-0.97, P-Value < 2.2e-16) (Fig. S8. J).

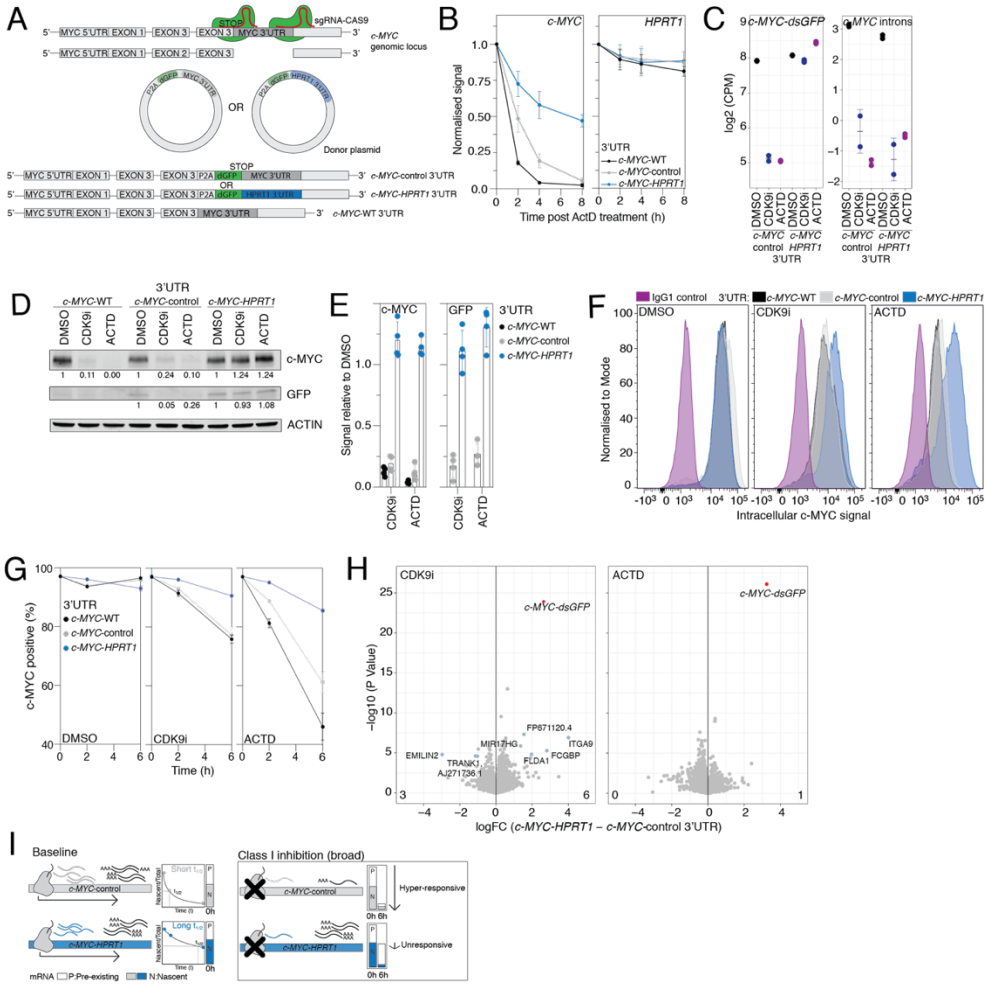

Figure 6 Increased *c-MYC* RNA stability renders it less sensitive to transcriptional targeting
(A) Schematic of CRISPR/Cas9 -homology directed repair (HDR) used to endogenously swap the *c-MYC* 3' untranslated region (3'UTR) for the *HPRT1* 3'UTR in the K562 cell line. **(B)** Normalized expression of ***(left)*** *c-MYC* and ***(right)*** *HPRT1* transcripts following the addition of ACTD at indicated time points as measured by quantitative real time PCR (qRT-PCR). Values are mean with error bars representing standard deviation (sd) of three biological replicates from three separate single cell clones. **(C)** ***(Left)*** Total gene expression of reads mapping across *c-MYC* and *dsGFP* sequences with indicated treatments and cell lines after 6 hours. ***(Right)*** *c-MYC* intron expression with indicated treatments and cell lines after 6 hours. **(D)** Western blot of ***(top)*** c-MYC, ***(middle)*** GFP and ***(bottom)*** ACTIN protein with indicated treatments and cell lines after six hours. Values indicated are protein levels normalized to ACTIN and DMSO controls. **(E)** Western blot protein signal of ***(left)*** c-MYC and ***(right)*** GFP relative to ACTIN and DMSO controls after 6 hours of treatment. Values are mean with error bars representing sd of three biological replicates. **(F)** Representative histogram of intracellular c-MYC protein staining following 6 hours of indicated treatments. **(G)** Proportion of cells positive for intracellular c-MYC protein staining following 0, 2 and 6 hours of indicated treatments. Values are normalized to 0-hour time point and are mean with error bars representing sd of two biological replicates. **(H)** Scatter plot of significance and difference in total gene expression with ***(left)*** CDK9i and ***(right)*** ACTD treatment between *c-MYC*-control and -*HPRT1* 3'UTR cell lines. **(I)** Simplified schematic of transcriptional responses with class I (selective) and class II (broad) inhibitors of *c-MYC* chimeric loci.

Prolonged *c-MYC* mRNA half-life did not rescue the expression of previously defined *c-MYC* target genes following transcriptional inhibition as assessed by nascent and total mRNA abundance [32] (Fig. S8. K, L). Although nascent *c-MYC* target gene expression was significantly less down-regulated with CDK9i treatment in the c-*MYC*-*HPRT1* 3'UTR cell line (Fig. S8. L), it was not sufficient to prevent reductions in total mRNA (Fig. S8. K), suggesting that class I inhibitors can perturb the expression of *c-MYC*-dependent targets independently from sustained *c-MYC* expression. Moreover, this also indicates that *c-MYC* driven

transcription itself may be inherently reliant on the molecular level on core-transcriptional components.

Taken together, these data show that swapping the *c-MYC* 3'UTR to the 3'UTR of a long-lived gene within its endogenous chromatin context, preserves the targeting of *de novo* mRNA production in response to transcriptional inhibitors, but renders *c-MYC* insensitive to transcriptional targeting when assessing total mRNA levels due to its increased transcript stability (Fig. 5I). Gene-intrinsic RNA decay properties are therefore a key determinant in establishing gene responsiveness to compounds that target RNAPII driven gene expression, and without which, selective responses would not be found with most transcriptional compounds (Fig. 7).

Discussion

RNAPII-driven transcription has been therapeutically targeted in oncology with biological and therapeutic effects proposed to occur through selective perturbation of oncogenic gene networks [1,20]. The current literature suggests that the discrete targeting of selected genes following transcriptional perturbation is mechanistically linked to association with SEs and disproportionate occupancy of critical chromatin co-factors, such as BRD4, at promotors; however, the role of RNA stability has not been extensively assessed in this context.

Here, we demonstrate that selective and broad targeting of RNAPII-driven transcription by class I and II therapeutic inhibitors, respectively, results in discrete alterations in total mRNA abundance that are defined by transcript decay rates (Fig. 7). Both class I and II inhibitors reduce the total mRNA levels of genes with short transcript half-lives, several of which are CR TFs, associated with oncogenic signaling pathways or promotor proximal to SEs. Although some studies indicate that these oncogenic networks are particularly sensitive due to reduction of the CR TFs within SE and promotor regions, whether down-regulation of TFs and SE-driven transcription were causally linked remained unclear [20,38,58]. Our data indicates that targeting of SE-driven transcription is only possible when the associated gene has short-lived RNA, and therefore implicates gene-intrinsic RNA decay parameters in the selective perturbation of SE oncogenic programs. In contrast, genes with stable RNAs are largely refractory to transcriptional targeting when assessing total RNA levels and are functionally related to cellular housekeeping roles [26,59]. This may prove a challenge for the use of transcriptional inhibitors as a therapeutic intervention for cancers that exhibit dysregulated metabolic activity or a heightened dependence on metabolic pathways.

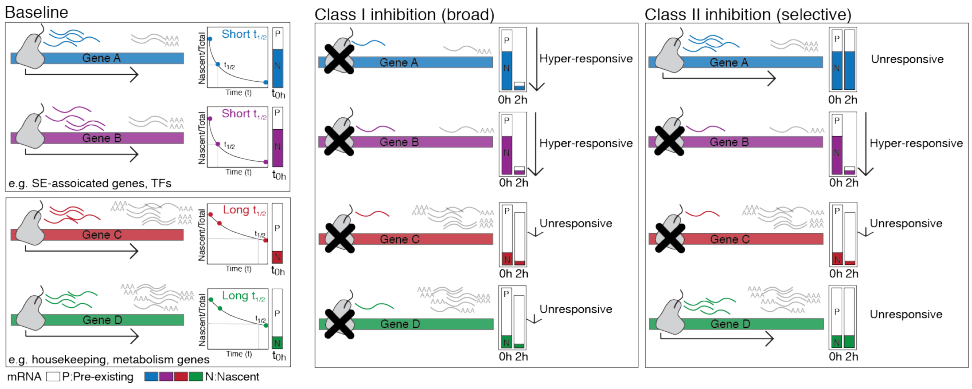

Figure 7 Simplified schematic of transcriptional responses of genes with short and long RNA half-lives with class I (selective) and class II (broad) inhibitors.

Transcript half-lives are strongly related to gene function [60]. For example, short-lived mRNA tend to be expressed from genes encoding chromatin co-factors, TFs, cytokines, cell-cycle and mitosis regulators [26,59,60]. As short-lived transcripts are able to be more rapidly induced and cleared in comparison to stable mRNA, it has been suggested that they have evolved to enable acute alterations of total mRNA levels [61]. This is critical for biological processes such as transcription, cellular proliferation and inflammation, which without rapid modulation and proper control can lead to cellular transformation and inappropriate immunological responses [55,62,63]. Maintenance of the steady state abundance of short-lived transcripts requires high RNA production rates [61]. It has been postulated that in cancer, genes encoding CR TFs have evolved and acquired SEs to drive their high-level production, and therefore are increased in their sensitivity to transcriptional perturbation [1]. An association between sensitive genes and these elements may therefore not be causal, but may rather be a consequence of the constant need to synthesize *de novo* RNA due to gene-intrinsic short half-lives.

Outside of the cancer context, transcriptional and epigenetic inhibitors have been employed as immunomodulatory and anti-inflammation agents. This includes as therapies to reduce PD-L1 expression and promote host anti-tumour responses [64–66], downregulate cytokine signalling pathways such as NFkB and TGF-β in rheumatic diseases [67–70] and repress pro-survival apoptotic proteins in arthritis [71]. In addition to their tumour intrinsic effects, transcriptional and epigenetic inhibitors also impact immune cells and their micro-environment directly [72,73]. Similar to our observations in tumour cell targeting, RNA half-life may have a significant role in determining the therapeutic outcome of transcriptional and epigenetic compounds in the aforementioned diseases contexts. Indeed, our data indicates that short-lived transcripts are also strongly related to inflammatory and cytokine pathways.

Interestingly, alterations in RNA decay frequently occur in cancer in either a gene-specific manner or through mutations in RNA complexes to thus affect global RNA turnover [55,62,74–76]. For example, stabilization and the resultant increase in steady state expression of the *PD-L1* transcript frequently occurs in haematological and stomach cancers from mutations that disrupt the *PD-L1* 3'UTR, and in *in vivo* models of lymphoma, leads to immune evasion and decreased survival [55]. Similarly, c-MYC 3'UTR truncations caused by chromosomal translocations in human T-cell leukaemias (TCL) have been described to increase c-MYC expression via transcript stabilisation [77,78]. In addition to gene-specific truncations of 3'UTR sequences in cancer, RNA stability can be broadly affected via genetic alterations that impact the RNA decay machinery and RNA Binding Proteins (RBPs). This includes loss of function mutations in the Carbon Catabolite Repression—Negative On TATA-less (CCR4-NOT) Transcription subunit 3 (CNOT3) subunit of the CCR4-NOT deadenylase complex in T-cell Acute Lymphoblastic Leukaemia (T-ALL),[74] and the 3'-5' exoribonuclease of the exosome complex, DIS3 in MM and RUNX1 -mutated AML[75,76]. Moreover, widespread alternative polyadenylation (APA) in a variety of cancer types has been demonstrated to shorten 3'UTRs and increase transcript stability and protein levels [62,79]. Whilst the mechanism of increased APA in cancers is poorly understood, there is evidence that down-regulation APA factors such as CFIm25 and PCF11 may contribute increased APA in certain malignancies [80]. Based on our observations that long-lived transcripts are resistant to transcriptional inhibition, targeting stabilized oncogenic RNA in the context of deregulated decay machinery may prove unsuccessful with class I and II therapeutic compounds. To our knowledge, the therapeutic targeting of RNA decay in the oncology setting

remains largely unexplored. An exception to this is MS-444, which inhibits HuR/ELAVL1, an RBP that has been associated with proto-oncogenic roles due to its ability to stabilize tumorigenic transcripts that contain AREs [81–83] Having observed that a large number of RNAs are not sensitive to transcriptional perturbation due to their long half-lives (Fig. 1-4), combination therapy with a transcript destabilizing agent such as MS-444 provides a novel opportunity to target genes that were otherwise impervious to RNAPII targeting.

Overall, this study highlights the importance of RNA decay parameters in governing total gene expression levels in response to selective and global inhibitors of RNAPII -driven transcription, and provides novel mechanistic insight that can be leveraged for therapeutic benefit. Moreover, our work shifts the paradigm that selective responses observed in these contexts are largely driven by selective abrogation of RNA synthesis as a result of particular genomic determinants but rather demonstrates that these largely result from gene-intrinsic RNA properties.

MATERIALS AND METHODS

Cell lines and culture

K562 CML parental and HDR-edited and THP-1 AML cells were cultured in RPMI 1640 (Thermo Fisher Scientific, Waltham, MA, USA, 11875093) containing 10% (v/v) heat-inactivated fetal bovine serum (HI-FBS; Thermo Fisher Scientific, 10099), penicillin (100 U/ml), streptomycin (100 µg/ml) (Thermo Fisher Scientific, 15140122) and 2 mM GlutaMAX (Thermo Fisher Scientific, 35050061) at 37°C and 5% carbon dioxide. Drosophila melanogaster S2 cells were cultured Schneider's *Drosophila* medium (Thermo Fisher Scientific, 21720) supplemented with 10% HI-FBS, penicillin (100 U/ml), streptomycin (100 µg/ml), and 2 mM GlutaMAX at room temperature and atmospheric carbon dioxide. Cell lines for all assays were seeded at 50-70% confluency the day prior unless otherwise indicated.

Compounds

See supplementary tables 1 and 2.

CRISPR HDR generation of MYC transcript stable clones

Parental K562 cells (5e+05) were washed in Phosphate Buffered Saline (PBS) twice and resuspended in Cell Line Nucleofector solution SF (16.4uL) with Supplement (3.6uL) (SF Cell Line 4D-nucleofector X Kit, Lonza, V4XC-2032). Alt-R SpCas9 nuclease (100pmol, Integrated DNA Technologies, 1074182), single guide RNAs (sgRNAs) targeting the c-MYC stop codon and 3' end of its 3'UTR (300pmol, supplementary table 3) and pUC57 or pUC57-Mini donor plasmid (1000ng; GenScript Gene Sythesis) containing recombinant sequences for dGFP, P2A cleavable peptide and HPRT1 or c-MYC 3'UTRs, respectively (supplementary table 4), were incubated together for 20 minutes at room temperature, prior to being placed on ice. Ribonucleoprotein (RNP) complex (5uL) was added to the cell suspension (20uL), 20uL of which was subsequently transferred to 16-well Nucleocuvette Strip and electroporated using the 4D-Nuceleofector X unit (program FF120, Lonza, AAF-1002X). Warmed culture medium (100uL) was added to cell suspension and incubated at 37°C and 5% carbon dioxide for 10 minutes. Cell suspension was then transferred to a 24-well cell culture plate containing culture medium (1mL) and IDT Alt-R HDR electroporation enhancer (20uM; Integrated DNA Technologies, 1081073) and incubated at 37°C and 5%

carbon dioxide for 24 hours, after which cells were washed twice with fresh culture medium and cultured at 37°C and 5% carbon dioxide. After expansion, cells were sorted and enriched for GFP positivity three successive times, followed by isolation of single cells into 96-well culture plates using Becton Dickinson (BD) FACSAria Fusion 3 or 5 Cell Sorters. Three clones with successful knock in of each donor vector were identified with KAPA HiFi (Roche, 7958935001) using isolated genomic DNA (DNeasy Blood & Tissue Kits (Qiagen, 69506) and primers designed outside or within plasmid homology arms (supplementary table 5). PCR fragments were subsequently separated using agarose gel electrophoresis (see below). Knock-in sequence was validated using Sanger sequencing of PCR fragments detailed above at the Australian Genome Research Facility (AGRF). Total-RNA sequencing was performed using a single representative clone of each knock-in.

Agarose gel electrophoresis and gel imaging

Blue/orange loading dye 6X (Promega, G1881) was added to PCR fragments, which were subsequently separated using 1% agarose gels prepared with molecular grade agarose (Bioline, BIO-41025), Tris base-acetic acid- EDTA (TAE) 1X solution and SYBR Safe DNA Gel Stain (Life Technologies, S33102). Agarose gels were imaged on the GelDoc XR+ Imager (BioRad) using ImageLab Software (BioRad).

Propidium Iodide and Cell Trace Violet staining

Cells (1e+07) were centrifuged (1400rpm at 4°C for 4 minutes), resuspended in PBS supplemented with 0.1% (w/v) BSA and stained with 5uM Cell Trace Violet (CTV) dye (Thermo Fisher Scientific, C34557) in a 37°C water bath for 10 minutes. Five volumes of ice-cold culture medium was added to cell suspension to quench unbound dye. Cells were then centrifuged (1400rpm at 4°C for 4 minutes), resuspended in PBS supplemented with 2% (v/v) HI-FBS, sorted for CTV-positivity on BD FACSAria Fusion 3 or 5 Cell Sorters and treated with ultrapure water or 4-sU for 24 hours. Following treatment, cells were incubated in PBS containing 1ug/mL Propidium Iodide (PI) (Sigma Aldrich, P4170) and analysed using the BD Fortessa X20. FlowJo v10 software (Ashland) was used to analyse flow cytometric data.

Quantitative PCR and analysis

Cells (1e+06 per time point) were incubated with 1ug/mL ACTD at 37°C and 5% carbon dioxide, harvested 0-, 2-, 4- and 8- hours post-treatment, centrifuged (1400rpm at 4°C for 4 minutes), washed in ice-cold PBS and resuspended in 300uL TRIzol (Thermo Fisher Scientific, 15596026). RNA was extracted from lysates using the Direct-zol RNA MiniPrep Kit (Zymo Research, R2052) and complimentary DNA (cDNA) was synthesised (from 1ug RNA) using the Applied Biosystems High Capacity cDNA Reverse Transcription Kit (Thermo Fisher Scientific, 4368814). Quantitative PCR (qPCR) was performed using cDNA, 0.25uM forward and reverse oligo primers (see supplementary table 6) and SensiFAST SYBR Hi-ROX Kit (Bioline, BIO-92005) in 384-well plates with the LightCycler 480 Instrument II (Roche, 05015243001). Threshold cycles for each reaction were analysed using the $\Delta\Delta C_t$ method normalising to GAPDH as the housekeeping gene.

SDS-polyacrylamide gel electrophoresis and western blotting

Cells (1e+06) were washed in PBS, lysed in Laemelli Buffer (60 mM tris-HCl (pH 6.8), 10% (v/v) glycerol, and 2% (w/v) SDS) and incubated at 95°C for 10 minutes. Lysate protein concentration was determined using the Pierce BCA Protein Assay Kit (Thermo Fisher Scientific, 23225) and absorbance at 562nm

wavelength was measured on the iMark Microplate Absorbance reader (BioRad) using MicroPlate Manager Software (BioRad). 20 X sample buffer (100 % β-mercaptoethanol, and bromophenol blue) was added to lysates and were subsequently incubated for an additional 5 minutes. Lysates were separated using Mini-PROTEAN TGX 4 to 15% gradient gels (25 mM tris, 192 mM glycine, and 0.1% (w/v) SDS; Bio-Rad, 4561086) and transferred at 4°C to either Immobilon-FL or Immunoblon-P (IPVH00010) polyvinylidene fluoride membranes (Merck, IPFL00010) (1.5 hours; 250 mA, 25 mM tris, 192 mM glycine, and 5% (v/v) methanol).

Immobilon-FL membranes were dried for 1 hour at room temperature, washed in ultrapure water, 100% methanol, Tris buffered saline (TBS) in the listed order and blocked using Odyssey blocking buffer (Li-COR, 927-40000). They were then incubated in primary antibodies (supplementary table 7) diluted in Odyssey blocking buffer supplemented with 0.2% (v/v) Tween 20 (Sigma-Aldrich, P9416) overnight at 4°C, washed three times with TBS containing 0.1% (v/v) Tween 20 and incubated with IRDye-conjugated secondary antibodies (supplementary table 7) diluted in Odyssey blocking buffer supplemented with 0.2% (v/v) Tween 20 and 10% (v/v) sodium dodecyl sulfate (SDS) for 1 hour at room temperature. Immobilon-FL membranes were washed in PBS and protein was visualised and quantified using the Odyssey CLx and Image Studio Lite software 2 (Li-COR).

Immunoblon-P membranes were blocked in TBS supplemented with 5% (w/v) skim milk powder and Tween 20, incubated with primary antibodies (supplementary table 7) diluted in the same solution at 4°C overnight, washed three times with TBS containing 0.1% (v/v) Tween 20 and incubated with horseradish peroxidase-conjugated secondary antibodies (supplementary table 7) at room temperature for 1 hour. Protein was subsequently visualised using Amersham ECL Plus (GE Healthcare, RPN2132) and Super RX film (Fujifilm, 03G01).

Intracellular staining of c-MYC

Intracellular staining of Myc was performed as previously described [1]. Briefly, cells were harvested at the timepoints indicated and were immediately resuspended in fixation buffer (0.5% paraformaldehyde, 0.2% Tween-20 and 0.1% bovine serum albumin in PBS) at room temperature, for at least 24 hours until staining was performed. Fixed cells were stained with either anti-Myc (clone D84C12, Cell Signalling Technology) or a rabbit IgG isotype-matched control antibody (clone D1AE, Cell Signalling Technology) before staining with an anti-rabbit IgG conjugated to Alexa Fluor 647. Staining of all fixed samples within one experiment was performed at the same time.

Total RNA-sequencing

Cells (1e+06[6] per treatment condition) were centrifuged (1400rpm at 4°C for 4 minutes), washed in ice-cold PBS and resuspended in 350µl of Buffer RLT Plus supplemented with 1% (v/v) β-mercaptoethanol from the RNeasy Plus Mini Kit (Qiagen, 74134). RNA was extracted using the same kit according to manufacturer's instructions and quality was assessed using the Agilent 2200 TapeStation System (Agilent, G2964AA) with RNA ScreenTape (Agilent, 5067-5576) and Sample Buffer (Agilent, 5067-5577). S2 spike-in material (5%) was added to RNA. Sequencing libraries were prepared using NEBNext Ultra II Directional RNA Library Prep Kit for Illumina, where ribodepletion was performed using the NEBNext rRNA Depletion Kit (New England BioLabs, E6310). Paired-end 75 base pair (bp) reads were sequenced using the NextSeq 500 (Illumina).

SLAM-sequencing

Protocol was adapted from [2]. K562 and THP-1 cells (1e+06 per treatment) were first pre-treated with small molecule inhibitors for a total time of 2 hours to pre-establish protein-target inhibition. Newly synthesized RNA in K562 cells was then labelled using 100 μM 4-sU in the final 1 hour of treatment at 37°C and 5% carbon dioxide. Cells were washed in ice-cold PBS and resuspended in 300μL TRIzol. For direct measurement of RNA half-lives, newly synthesized RNA was labelled by incubating cells in 30μM 4-sU for 12 hours at 37°C and 5% carbon dioxide, whereby culture medium was exchanged every 3 hours for the duration of the pulse. For the uridine chase, cells were centrifuged (1400rpm at 4°C for 4 minutes), washed in sterile ice-cold PBS twice and resuspended in pre-warmed (37°C) culture medium containing 3mM uridine (Sigma Aldrich, U6381). At 0- ,1-, 2-, 4-, 8-, 12- hours for K562 cells and 0-, 0.3-, 0.6-, 1-, 2-. 4-, 8- hours for THP-1 cells post the uridine chase, cells were harvested, centrifuged (1400rpm at 4°C for 4 minutes) and resuspended in 300μL TRIzol. For treatment-specific RNA decay rates, cells were centrifuged (1400rpm at 4°C for 4 minutes), washed in sterile ice-cold PBS twice and resuspended in pre-warmed (37°C) culture medium containing 3mM uridine (Sigma Aldrich, U6381) and either 1μM DMSO, JQ1 or AZ-5576. At 0-, 2-, 4- and 8- hours post uridine chase/drug addition, cells for each treatment condition were harvested, centrifuged (1400rpm at 4°C for 4 minutes) and resuspended in 300μL TRIzol. All SLAM-seq experiments included a non- 4-sU labelled control unless otherwise stated. To extract RNA, one-fifth volume of chloroform was added to TRIzol lysates, followed by shaking, incubation at room temperature for 2 minutes and centrifugation (16000g at 4°C for 15 minutes). The aqueous phase was isolated and RNA was precipitated using DTT (10mM), 100% isopropanol (1 volume) and GlycolBlue co-precipitant (15ug, Ambion, AM9515), incubated at room temperature for 10 minutes and centrifuged (16000g at 4°C for 20 minutes). Supernatant was removed, RNA pellets were washed in 75% (v/v) ethanol and DTT (100μM) and centrifuged (7500g at room temperature for 5 minutes). Supernatant was removed and RNA pellets dried for 10 minutes prior to reconstitution in Ultrapure DNAse/RNAse-free distilled water (Thermo Fisher Scientific, 10977023) supplemented with DTT (1mM) and incubation at 55°C for 10 minutes. Thiol-containing bases were reduced by incubating RNA (10μg) with IAA (10mM, 50 mM $NaPO_4$ pH 8.05 and 50% (v/v) DMSO) in a final volume of 50μL for 15 minutes at 55°C. Reaction was stopped by quenching IAA with DTT (20μM). RNA was precipitated using 3M NaOAc pH 5.2 (5μL), 100% ethanol (125μL) and GlycolBlue co-precipitant, incubated at -80°C for 30 minutes and centrifuged (16000g at 4°C for 30 minutes). Supernatant was removed and RNA pellet was washed in 75% (v/v) ethanol and centrifuged (16000g at 4°C for 10 minutes) twice, dried at room temperature for 10 minutes and reconstituted in Ultrapure DNAse/RNAse-free distilled water. RNA clean-up was performed by incubating RNA solution in 2 volumes of AMPure XP Beads (Beckman Coulter, A63881) for 2 minutes at room temperature. Beads were washed in 80% (v/v) ethanol twice, dried at room temperature for 3 minutes and resuspended in Ultrapure DNAse/RNAse-free distilled water. Eluate was collected and RNA quality and concentration was assessed using the Agilent 2200 TapeStation System (Agilent, G2964AA) with RNA ScreenTape (Agilent, 5067-5576) and Sample Buffer (Agilent, 5067-5577). S2 spike-in material (5%) was added to RNA. Sequencing libraries were prepared using the QuantSeq 3′mRNA-seq Library Prep Kit FWD for Illumina (Lexogen, Vienna, Austria) and sequenced as single-end 75 base pair reads using the NextSeq 500 (Illumina).

TT-sequencing

Protocol is adapted from [3]. Cells (5e+07 per treatment condition) were incubated with 1mM 4sU for either 5 or 15 minutes at 37°C and 5% carbon dioxide, centrifuged (1400rpm at 4°C for 5 minutes) and resuspended in TRIzol (5mL). One-fifth volume of chloroform was added to lysates, followed by shaking, incubation at room temperature for 2 minutes and centrifugation (13000g at 4°C for 10 minutes). The aqueous phase was isolated and RNA was precipitated using 100% isopropanol (1 volume), incubated at room temperature for 10 minutes and centrifuged (13000rpm at 4°C for 10 minutes). Supernatant was removed and RNA pellet was washed in 70% (v/v) ethanol, reconstituted in Ultrapure DNAse/RNAse-free distilled water (100µL) and denatured at 65°C for 10 minutes. S2 spike-in (15µg) was added to RNA (150µg), material was adjusted to a final volume 100µL and sonicated in microTUBE AFA Fiber screw cap tubes (6 mm × 16 mm, Covaris, 520096) using the Covaris S220 Focused-ultrasonicator at a maximum power for 15 seconds. Thiol-specific biotinylation of RNA was performed in a final volume of 1.5mL by incubation with 10 mM tris (pH 7.4), 1 mM EDTA, 20% (v/v) dimethylformamide (200 µg/ml; Sigma-Aldrich, 227056), and 300 µg of EZ-Link HPDP-Biotin (Thermo Fisher Scientific, 21341) for 1.5 hours at room temperature. An equal volume of chloroform was added to reaction, followed by shaking, incubation at room temperature for 2 minutes and centrifugation (1400rpm at 4°C for 5 minutes). Aqueous phase was isolated and an equal volume of chloroform was added, followed by shaking, incubation at room temperature for 2 minutes and centrifugation (1400rpm at 4°C for 5 minutes). This step was repeated an additional one time. Aqueous phase was isolated and RNA was precipitated using 5M NaCl (10% volume) and 100% isopropanol (1 volume) and centrifugation (20000g at 4°C for 20 minutes). RNA pellets were washed in 75% (v/v) ethanol, reconstituted in Ultrapure DNAse/RNAse-free distilled water (100µL) and denatured at 65°C for 10 minutes. Biotinylated RNA was separated from the total RNA pool by incubation with streptavidin beads (µMACs Streptavidin Kit, Miltenyi Biotec, Bergisch Gladbach, Germany, 130-074-101) at room temperature for 15 min with constant rotation. µMACs columns pre-equilibrated with room temperature wash buffer (100 mM tris-HCl (pH 7.4), 10 mM EDTA, 1 M NaCl, and 0.1% (v/v) Tween 20) were used to bind streptavidin beads, which were then washed using 900µL wash buffer that was heated to 65 °C or at room temperature, 5 times each. Biotinylated RNA was eluted into 700µL Buffer RLT from the RNeasy MinElute Cleanup Kit (Qiagen, 74204) through two additions of 100 mM DTT (100µl) 3 min apart, and then isolated using the same kit according to manufacturer's instructions. RNA concentration was quantified using the Agilent 2200 TapeStation System (Agilent, G2964AA) with High Sensitivity RNA ScreenTape (Agilent, 5067-5579) and Sample Buffer (Agilent, 5067-5580).
Sequencing libraries were prepared with the NEBNext Ultra II Directional RNA Library Prep Kit for Illumina (without additional fragmentation), where ribodepletion was performed using the NEBNext rRNA Depletion Kit (New England BioLabs, E6310). Single-end 75 base pair reads were sequenced using the NextSeq 500 (Illumina).

MAC-seq

Cells (5e+04 per well) in a final volume of 100µL in a 96-well plate format were incubated with transcriptional and epigenetic inhibitors in technical duplicate for 6 hours (supplementary table 8) at 37°C and 5% carbon dioxide. 5e+03 cells from each well were aliquoted into a separate 96-well plate, washed in ice-cold PBS twice and centrifuged (1400rpm at 4°C for 4minutes). Supernatant was removed and cell pellets were frozen at -80°C. Library preparation is adapted from [4]. In detail, 17 µl lysis buffer were added into each well of a 96-well plate containing cell pellets and incubated at room temperature for 15 min under agitation (900 rpm). 12.5 µl of cell lysate were transferred into each well of a new 96-well plate previously

prepared with 1 µl of 10 nM well-specific RT MAC-seq primer and 7.5 µl RT mix; the RT mix contains a TSO primer and external ERCC RNAs. The mixture was incubated for 2 hours at 42 C to create well-barcoded full length cDNA and then all the wells of a plate were combined into a single tube. Concentration and clean-up was done via column purification (DNA Clean and Concentrator™-100, Zymo Research) and RNAClean XP beads (Beckman Coulter) and each plate eluted in 22 µl nuclease free water. The purified cDNA was pre-amplified with KAPA HiFi HotStart ReadyMix (Roche) and MAC-seq PreAmp PCR primer and the quality checked on a D5000 Screentape (TapeStation, Agilent). One barcoded library was prepared per plate using TD buffer and TDE1 enzyme (Illumina) for tagmentation and KAPA HiFi HotStart Ready Mix (Roche) and custom primers (MAC-seq P5 PCR and MAC-seq Indexing Mix) for amplification. Libraries were purified with DNA Ampure XP beads (Beckman Coulter), quality checked on a DNA1000 tape (TapeStation, Agilent) and quantity verified by qPCR. Two indexed libraries were sequenced on a NextSeq 500 instrument (Illumina) using a custom sequencing primer (MAC-seq Read primer) and a High Output Kit v2.5 75 Cycles (Illumina) with paired-end configuration (25 base pairs for read 1 and 50 base pairs for read 2).

SLAM-seq analysis

Single-end reads were demultiplexed using bcl2fastq (v2.17.1.14) and resulting FASTQ files were trimmed for adapter sequences using Trim_galore (v0.6.5) with a stringency overlap of 3bp. Trimmed FASTQ files were processed with SLAM-dunk (v0.4.3), enabling multi-mapper reconciliation and using a threshold of at least 2 T > C conversions to mark a read as converted. The no 4sU control sample was processed first to find single nucleotide polymorphisms (SNPs), which was then used to filter the subsequent samples. `bedtools merge` was then used to merge the 3' UTRs of each Ensembl transcript by gene (v77 identifiers for hg38) for use in the SLAM-dunk counting step. The Broad Institute GSEA software was used to perform GSEA [5]. Differential gene testing was performed on counts normalized to library sizes scaled to external S2 spike-ins and filtered for lowly expressed genes using edgeR (v3.32.1) on Rstudio (v4.0.2). SLAM sequencing tcount files from [6] (GEO accession GSE138210) and [7] (GEO accession GSE111463) were downloaded and differential gene testing was performed as described above.

TT-seq analysis

Single-end reads were demultiplexed using bcl2fastq (v2.17.1.14) and resulting FASTQ files were aligned to the genome using STAR (v2.7), which were then summarized using featureCounts in Subread (v2.0.1): counting reads with a minimum Mapping Quality Score (MQS) of 7 in the union of all transcript isoforms of each Ensembl gene. Only genes with at least 10 reads per million across at least two samples within an experiment were retained for further analysis. In order to compare expression levels between samples, raw read counts for each gene were converted to reads per million using adjusted library sizes calculated with edgeR's TMM implementation on the spike-in read counts.

Total RNA-seq analysis

Paired-end reads were demultiplexed using bcl2fastq (v2.17.1.14) and resulting FASTQ files were quality checked using fastqc (v0.11.6), trimmed 15 bp from the 5' end to remove primer bias and filtered for quality and length using cutadapt (v2.1; -u 15 -U 15 -q 15 --pair-filter any --minimum-length 50). Trimmed reads were mapped to GRCh38/hg38 and BDGP6/dm6 genomes using hisat2 (v2.1.0) with paired read settings and resulting SAM files were converted to BAM files using samtools (v1.9; view), which were then sorted

and indexed. Reads mapping to either exonic or intronic genomic intervals were counted using a combined hg38/dm6/GFP GTF file with FeatureCounts from the subread package (v2.0.0; featureCounts -O -M -T 32 -p -s 2). Differential gene testing was performed on counts normalized to library sizes scaled to external S2 spike-ins and filtered for lowly expressed genes using edgeR (v3.32.1) on Rstudio (v4.0.2). Gene Ontology analysis was performed using the ToppGene suite [8–10].

MAC-seq analysis

Paired-end reads were demultiplexed using bcl2fastq (v2.17.1.14) and resulting FASTQ files were quality checked using fastqc (v0.11.6) and read 2 (R2) was trimmed 15 bp from the 5' end to remove primer bias using cutadapt (v2.1; -u 15). R2 FASTQ files of paired-end reads were demultiplexed according to well barcodes (supplementary table 9) and filtered for PCR duplicates using Unique Molecular Identifiers (UMIs), both present in read 1 (R1) using the scruff [11] R (v4.0.2) package dumultiplex function (bcStart = 1, bcStop = 10, bcEdit = 0, umiStart = 11, umiStop = 20, keep = 35, minQual = 20, yieldReads = 1e+06). R2 FASTQ files were then mapped to the GRCh37/hg19 genome and ERCC sequences using alignRsubread (unique = FALSE, nBestLocations = 1, format = "BAM") and resulting BAM files were used to count unique R2 reads mapping to exonic genomic intervals and ERCC sequences using a combined hg19/ERCC GTF file with countUMI (umiEdit = 0, format = "BAM", cellPerWell = 1. Both functions are from the scruff R package. Gene expression counts were normalized to library size and reads mapping to ERCC spike-ins using the RUVseq R package (v1.24.1). Subsequent count processing was performed using the Seurat R package (v3.2.1) [12], where lowly expressed genes were filtered and counts were normalized for latent variables including plate, well row and column, using the SCTransform function. SCTransformed scaled gene RNA expression values were then used for PCA, where shared-nearest-neighbours (SNN) network was calculated using the top 10 Principal Components with the FindNeighbours function using default parameters. Drug-treatment clusters were subsequently identified with the Louvain algorithm using a resolution parameter of 2. Uniform Manifold Approximation and Projection (UMAP) values were also calculated using the top 10 Principal Components with the RunUMAP function using default parameters. Differential gene testing relative to treatment controls (DMSO or EtOH) was performed using a hurdle model (MAST) with un-scaled gene RNA expression counts, plate and column numbers as latent variables and a logFC threshold of 0 with the FindMarkers Function. Area Under the Curve (AUC) scores for each drug treatment and gene lists indicated was calculated using all expressed genes with the R AUCell Package (v0.10.0).

ChIP-seq analysis and super-enhancer identification

H3K27ac ChIP-seq FASTQ files (SRR1957037, SRR1957038, GEO Accession GSM1652918) were downloaded using sratoolkit (v2.9.0, fastq-dump --gzip --split-files), quality checked using fastqc (v0.11.6) and mapped to the GRCh37/hg19 genome using bowtie2 (v2.3.4.1) with paired end read settings. Resulting SAM files were converted to BAM files using samtools (v1.9; view), which were then sorted and indexed. Potential PCR duplicates were filtered using the MarkDuplicates function from picard (v2.6.0; REMOVE_DUPLICATES= true) and BAM files were converted to TDF files using igvtools (v2.3.95; count -z 5 -w 10). H3K27ac peaks were called relative to input using macs (v2.1.1; callpeak -f BAMPE -g hs -q 0.01 -call-summits –cutoff-analysis) and peaks within hg19 ENCODE blacklist regions (https://www.encodeproject.org/files/ENCFF356LFX/) were removed using bedtools (v2.27.1) intersect

function. Super-enhancer calling was performed using Ranking Ordering of Super-Enhancer (ROSE2) (v1.0.5; -c INPUT -g hg19 -t 2000 -s 12500) [13] and were annotated to genes according to "TOP GENE."

Coltron analysis

The coltron algorithm (v1.0.2) [14] was used to identify SE-associated TFs and regulatory networks using ROSE2-determined super-enhancer peaks and H3K27ac BAM signal with default parameters.

Determination of RNA synthesis and decay rates

Solving the first order differential equation in Fig. 2F yields an exponential function with parameters for the synthesis rate (k_1), decay rate (k_2) and initial quantity of RNA (M_0):

$M(t) = (M_0 - K) * e^{(-k_2*t)} + K$

where $K = k_1/k_2$ is the quantity at equilibrium.

To determine decay rates (k_2) for each gene, precision-weighted nonlinear regression was used to fit an exponential curve to the decreasing quantity of SLAM-seq labelled reads measured post-washout of 4sU. Assuming no synthesis of labelled reads post-washout ($k_1 = 0$) leaves one parameter for the starting RNA concentration, which was set to the initial data point at T = 0, and one for the decay rate, which was fit using MINPACK's (v1.2-1) Levenberg-Marquardt implementation in R.

Precision weights for the fit were estimated using local regression. The standard deviation between technical replicates for a given mean expression level in the baseline SLAM-seq dataset was modelled with R's `loess` implementation, and then applied to calculate weights for the other samples during fitting.

Synthesis rates were determined by dividing the TT-seq adjusted reads per million for each gene by the length and sampling time, producing a scaled FPKMh^{-1} averaged across replicates.

Predictions

Predictions were made with the model using the fitted rates and differing initial conditions, then compared against a separate dataset of total mRNA measurements at T = 2, 6h.

Parameters set for simulated results:

Simulated Result	**Decay rate (k_1)**	**Synth. rate (k_2)**	**Initial qty (M_0)**
Simulated total transcriptional shutdown	Fitted decay rate under drug	0	Baseline equilibrium

ACKNOWLEDGMENTS

We thank members of the Victorian Centre for Functional Genomics, Peter MacCallum Centre Molecular Genomics Core, Daniel Ho from Novartis and the other authors for their help during MAC-seq protocol implementation and Compounds Australia at Griffith University for their provision of specialized compound management and logistics research services to the project.

FUNDING

I.T. was supported by an Australian Government Research Training Scholarship. S.J.V. was supported by a Rubicon fellowship (NWO, 019.161LW.017), NHMRC EL1 fellowship (GNT1178339), and The Kids' Cancer Project. R.W.J was supported by the Cancer Council Victoria, National Health and Medical Research Council of Australia (NHMRC), and The Kids' Cancer Project. A.T.P. was supported by a

National Health and Medical Research Council (NHMRC) Senior Research Fellowship (1116955). B.F. and A.T.P. were supported by the Lorenzo and Pamela Galli Charitable Trust and the Galli Next Generation Discoveries Initiative. The Victorian Centre for Functional Genomics (K.J.S.) is supported by the Australian Cancer Research Foundation (ACRF). G.M.A. is supported by a PeterMac Foundation Grant (ID # 1739), Phenomics Australia (PA) through funding from the Australian Government's National Collaborative Research Infrastructure Strategy (NCRIS) program, the Peter MacCallum Cancer Centre Foundation and the University of Melbourne Research Collaborative Infrastructure Program (MCRIP). Equipment used for this work was funded by the (Australian Cancer Research Foundation (ACRF, Tumour Heterogeneity Program). The research benefitted by support from the Victorian State Government Operational Infrastructure Support and Australian Government NHMRC Independent Research Institute Infrastructure Support.

AUTHOR CONTRIBUTIONS

I.T. performed experiments, next generation sequencing analysis, data interpretation and wrote the manuscript. B.F. and A.T.P performed next generation sequencing analysis and computational modelling. Z.F. designed sgRNA and plasmid templates for CRISPR-HDR. S.G., D.Y., G.M.A. and K.J.S. optimized and performed MAC-seq. I.Y.K. performed Myc intracellular staining and analysis and was supervised by E.D.H. S.J.V. and R.W.J. performed data interpretation, study supervision and co-wrote the manuscript. All co-authors proof-read and edited the manuscript.

COMPETING INTERESTS

The Johnstone laboratory receives funding support from Roche, BMS, Astra-Zeneca and MecRx. RWJ is a shareholder and consultant for MecRx.

REFERENCES

1. Bradner, J. E., Hnisz, D. & Young, R. A. Transcriptional Addiction in Cancer. *Cell* **168**, 629–643 (2017).
2. Bywater, M. J., Pearson, R. B., Mcarthur, G. A. & Hannan, R. D. Dysregulation of the basal RNA polymerase transcription apparatus in cancer. *Nat. Rev. Cancer* **13**, (2013).
3. Villicaña, C., Cruz, G. & Zurita, M. The basal transcription machinery as a target for cancer therapy. (2014).
4. Laham-karam, N., Pinto, G. P., Poso, A. & Kokkonen, P. Transcription and Translation Inhibitors in Cancer Treatment. **8**, 1–24 (2020).
5. Puissant, A. *et al*. Targeting MYCN in neuroblastoma by BET bromodomain inhibition. *Cancer Discov*. (2013) doi:10.1158/2159-8290.CD-12-0418.
6. Bandopadhayay, P. *et al*. BET bromodomain inhibition of MYC-amplified medulloblastoma. *Clin. Cancer Res*. (2014) doi:10.1158/1078-0432.CCR-13-2281.
7. Lockwood, W. W., Zejnullahu, K., Bradner, J. E. & Varmus, H. Sensitivity of human lung adenocarcinoma cell lines to targeted inhibition of BET epigenetic signaling proteins. *Proc. Natl.*

Acad. Sci. U. S. A. (2012) doi:10.1073/pnas.1216363109.

8. Filippakopoulos, P. *et al*. Selective inhibition of BET bromodomains. *Nature* 1–7 (2010) doi:10.1038/nature09504.

9. Abedin, S. M., Boddy, C. S. & Munshi, H. G. BET inhibitors in the treatment of hematologic malignancies: Current insights and future prospects. *OncoTargets and Therapy* (2016) doi:10.2147/OTT.S100515.

10. Asangani, I. A. *et al*. Therapeutic targeting of BET bromodomain proteins in castration-resistant prostate cancer. *Nature* (2014) doi:10.1038/nature13229.

11. Chaidos, A. *et al*. Potentantimyeloma activity of the novel bromodomain inhibitors I-BET151 and I-BET762. *Blood* (2014) doi:10.1182/blood-2013-01-478420.

12. Winter, G. E. *et al*. Phthalimide conjugation as a strategy for in vivo target protein degradation. *Science (80-.).* **348**, 1376–1382 (2015).

13. Chung, C., Chandwani, R., Marazzi, I., Wilson, P. & Coste, H. Suppression of inflammation by a synthetic histone mimic. *Nature* **468**, 1119–1123 (2017).

14. Lasko, L. M. *et al*. Discovery of a selective catalytic p300/CBP inhibitor that targets lineage-specific tumours. *Nature* **550**, 128–132 (2017).

15. Galbraith, M. D., Bender, H. & Espinosa, J. M. Therapeutic targeting of transcriptional cyclin-dependent kinases. *Transcription* **10**, 118–136 (2019).

16. Bensaude, O. Inhibiting eukaryotic transcription: Which compound to choose? How to evaluate its activity? *Transcription* **2**, 103–108 (2011).

17. Baker, A. *et al*. The CDK9 inhibitor dinaciclib exerts potent apoptotic and antitumor effects in preclinical models of MLL-rearranged acute myeloid Leukemia. *Cancer Res*. (2016) doi:10.1158/0008-5472.CAN-15-1070.

18. Gregory, G. P. *et al*. CDK9 inhibition by dinaciclib potently suppresses Mcl-1 to induce durable apoptotic responses in aggressive MYC-driven B-cell lymphoma in vivo. *Leukemia* (2015) doi:10.1038/leu.2015.10.

19. Martin, R. D., Hébert, T. E. & Tanny, J. C. Therapeutic targeting of the general RNA polymerase II transcription machinery. *Int. J. Mol. Sci.* **21**, (2020).

20. Jia, Q., Chen, S., Tan, Y., Li, Y. & Tang, F. Oncogenic super-enhancer formation in tumorigenesis and its molecular mechanisms. *Exp. Mol. Med.* **52**, 713–723 (2020).

21. Lovén, J. *et al*. Selective inhibition of tumor oncogenes by disruption of super-enhancers. *Cell* (2013) doi:10.1016/j.cell.2013.03.036.

22. Chipumuro, E. *et al*. CDK7 inhibition suppresses super-enhancer-linked oncogenic transcription in MYCN-driven cancer. *Cell* **159**, 1126–1139 (2014).

23. Christensen, C. L. *et al*. Targeting Transcriptional Addictions in Small Cell Lung Cancer with a Covalent CDK7 Inhibitor. *Cancer Cell* (2014) doi:10.1016/j.ccell.2014.10.019.

24. Kwiatkowski, N. *et al*. Targeting transcription regulation in cancer with a covalent CDK7 inhibitor. *Nature* **511**, 616–620 (2014).

25. Laitem, C. *et al*. CDK9 inhibitors define elongation checkpoints at both ends of RNA polymerase II-transcribed genes. *Nat. Struct. Mol. Biol.* **22**, 396–403 (2015).

26. Herzog, V. A. *et al*. Thiol-linked alkylation of RNA to assess expression dynamics. *Nat. Methods* **14**, 1198–1204 (2017).

27. Lusser, A. *et al*. Thiouridine-to-Cytidine Conversion Sequencing (TUC-Seq) to Measure mRNA Transcription and Degradation Rates. *Methods Mol. Biol*. (2020) doi:10.1007/978-1-4939-9822-7_10.

28. Schofield, J. A., Duffy, E. E., Kiefer, L., Sullivan, M. C. & Simon, M. D. TimeLapse-seq: Adding a temporal dimension to RNA sequencing through nucleoside recoding. *Nat. Methods* **15**, 221–225 (2018).

29. Michel, M., Zacher, B., Demel, C., Tresch, A. & Gagneur, J. TT-seq maps the human transient transcriptome. *Science (80-.).* **352**, (2016).

30. Rabani, M. *et al*. Metabolic labeling of RNA uncovers principles of RNA production and degradation dynamics in mammalian cells. *Nat. Biotechnol*. **29**, (2011).

31. Duffy, E. E. *et al*. Tracking Distinct RNA Populations Using Efficient and Reversible Covalent Chemistry Technology Tracking Distinct RNA Populations Using Efficient and Reversible Covalent Chemistry. *Mol. Cell* **59**, 858–866 (2015).

32. Muhar, M. *et al*. SLAM-seq defines direct gene-regulatory functions of the BRD4-MYC axis. *Science (80-.).* **360**, 800–805 (2018).

33. Mertz, J. A. *et al*. Targeting MYC dependence in cancer by inhibiting BET bromodomains. *Proc. Natl. Acad. Sci. U. S. A.* **108**, 16669–16674 (2011).

34. Parua, P. K. *et al*. A Cdk9-PP1 switch regulates the elongation-termination transition of RNA polymerase II. *Nature* **558**, 460–464 (2018).

35. Alexander J. Federation, Donald R. Polaski, C. J. O., Fan, A., Lin, C. Y., E., J. & Bradner. Identification of candidate master transcription factors within enhancer-centric transcriptional regulatory networks. *bioRxiv* (2018).

36. Yamada, T. & Akimitsu, N. Contributions of regulated transcription and mRNA decay to the dynamics of gene expression. *Wiley* 1–18 (2019) doi:10.1002/wrna.1508.

37. Wu, Q. *et al*. Translation affects mRNA stability in a codon-dependent manner in human cells. *Elife* 1–22 (2019).

38. Hnisz, D. *et al*. Super-enhancers in the control of cell identity and disease. *Cell* (2013) doi:10.1016/j.cell.2013.09.053.

39. Zuber, J. *et al*. RNAi screen identifies Brd4 as a therapeutic target in acute myeloid leukaemia. *Nature* **478**, 524–528 (2011).

40. Delmore, J. E. *et al*. BET bromodomain inhibition as a therapeutic strategy to target c-Myc. *Cell* **146**, 904–917 (2011).

41. Dawson, M. A. *et al*. Inhibition of BET recruitment to chromatin as an effective treatment for MLL-fusion leukaemia. *Nature* **478**, 529–533 (2011).

42. Chen, J., Xu, H., Aronow, B. J. & Jegga, A. G. Improved human disease candidate gene prioritization using mouse phenotype. *BMC Bioinformatics* **8**, 1–13 (2007).

43. Chen, J., Aronow, B. J. & Jegga, A. G. Disease candidate gene identification and prioritization using protein interaction networks. *BMC Bioinformatics* **10**, 1–14 (2009).

44. Chen, J., Bardes, E. E., Aronow, B. J. & Jegga, A. G. ToppGene Suite for gene list enrichment analysis and candidate gene prioritization. *Nucleic Acids Res*. **37**, 305–311 (2009).

45. Zhou, Y. *et al*. Metascape provides a biologist-oriented resource for the analysis of systems-level datasets. *Nat. Commun*. (2019) doi:10.1038/s41467-019-09234-6.

46. Gilan, O. *et al*. Selective targeting of BD1 and BD2 of the BET proteins in cancer and immunoinflammation. *Science (80-.)*. **368**, 387–394 (2020).

47. Timmers, H. T. M. & Tora, L. Transcript Buffering: A Balancing Act between mRNA Synthesis and mRNA Degradation. *Mol. Cell* **72**, 10–17 (2018).

48. Ye, C. *et al*. DRUG-seq for miniaturized high-throughput transcriptome profiling in drug discovery. *Nat. Commun*. 1–9 (2018) doi:10.1038/s41467-018-06500-x.

49. Chen, C. Y. A. & Shyu, A. Bin. AU-rich elements: characterization and importance in mRNA degradation. *Trends in Biochemical Sciences* (1995) doi:10.1016/S0968-0004(00)89102-1.

50. Grzybowska, E. A., Wilczynska, A. & Siedlecki, J. A. Regulatory Functions of 3′UTRs. *Biochem. Biophys. Res. Commun*. (2001) doi:10.1006/bbrc.2001.5738.

51. Lal, A. *et al*. miR-24 Inhibits Cell Proliferation by Targeting E2F2, MYC, and Other Cell-Cycle Genes via Binding to 'Seedless' 3′UTR MicroRNA Recognition Elements. *Mol. Cell* **35**, 610–625 (2009).

52. Sachdeva, M. *et al*. p53 represses c-Myc through induction of the tumor suppressor miR-145. *Proc. Natl. Acad. Sci. U. S. A*. **106**, 3207–3212 (2009).

53. Yeilding, N. M., Rehman, M. T. & Lee, W. M. Identification of sequences in c-myc mRNA that regulate its steady-state levels. *Mol. Cell. Biol*. **16**, 3511–3522 (1996).

54. Caput, D. *et al*. Identification of a common nucleotide sequence in the 3'-untranslated region of mRNA molecules specifying inflammatory mediators. *Proc. Natl. Acad. Sci. U. S. A*. (1986) doi:10.1073/pnas.83.6.1670.

55. Kataoka, K. *et al*. Aberrant PD-L1 expression through 3′-UTR disruption in multiple cancers. *Nature* **534**, 402–406 (2016).

56. Buffering, T., Act, B., Synthesis, R. N. A. & Degradation, R. N. A. Transcript Buffering : A Balancing Act between mRNA Synthesis and mRNA Degradation. *Mol. Cell* (2018) doi:10.1016/j.molcel.2018.08.023.

57. Jia, Y., Chng, W. J. & Zhou, J. Super-enhancers: Critical roles and therapeutic targets in hematologic malignancies. *J. Hematol. Oncol*. **12**, 1–17 (2019).

58. Gryder, B. E. *et al*. Chemical genomics reveals histone deacetylases are required for core regulatory transcription. *Nat. Commun*. **10**, 1–12 (2019).

59. Schwanhüusser, B. *et al*. Global quantification of mammalian gene expression control. *Nature* **473**, 337–342 (2011).

60. Ruzsics, Z., Koszinowski, U. H., Friedel, C. C., Do, L. & Zimmer, R. Conserved principles of mammalian transcriptional regulation revealed by RNA half-life. *Nucleic Acids Res*. **37**, (2009).

61. Alon, U. *An introduction to systems biology: Design principles of biological circuits. An Introduction to Systems Biology: Design Principles of Biological Circuits* (2006).

62. Mayr, C. & Bartel, D. P. Widespread Shortening of 3′UTRs by Alternative Cleavage and Polyadenylation Activates Oncogenes in Cancer Cells. *Cell* **138**, 673–684 (2009).

63. Colley, S. M., Tilbrook, P. A. & Klinken, S. P. Increased transcription of the Eμ-myc transgene and mRNA stabilisation produce only a modest elevation in Myc protein. *Oncogene* **14**, 2735–2739 (1997).

64. Zhu, H. *et al*. BET Bromodomain Inhibition Promotes Anti-Tumor Immunity by Suppressing PD-L1 expression. *Cell Rep*. **16**, 2829–2837 (2017).

65. Hogg, S. J. *et al*. BET-Bromodomain Inhibitors Engage the Host Immune System and Regulate Expression of the. *Cell Rep*. **18**, 2162–2174 (2017).

66. Zhang, H. *et al*. Targeting CDK9 Reactivates Epigenetically Silenced Genes in Cancer. *Cell* **175**, 1244-1258.e26 (2018).

67. Duan, Q. *et al*. BET bromodomain inhibition suppresses innate inflammatory and profibrotic transcriptional networks in heart failure. *Sci. Transl. Med*. **9**, 23–25 (2017).

68. Klein, K. Bromodomain protein inhibition: A novel therapeutic strategy in rheumatic diseases. *RMD Open* **4**, 1–10 (2018).

69. Rossi, A. G. *et al*. Cyclin-dependent kinase inhibitors enhance the resolution of inflammation by promoting inflammatory cell apoptosis. *Nat. Med*. **12**, 1056–1064 (2006).

70. Wang, K. *et al*. Cyclin-dependent kinase 9 activity regulates neutrophil spontaneous apoptosis. *PLoS One* **7**, 3–8 (2012).

71. Hellvard, A. *et al*. Inhibition of CDK9 as a therapeutic strategy for inflammatory arthritis. *Sci. Rep*. **6**, 1–11 (2016).

72. Hogg, S. J., Beavis, P. A., Dawson, M. A. & Johnstone, R. W. Targeting the epigenetic regulation of antitumour immunity. *Nat. Rev. Drug Discov*. **19**, 776–800 (2020).

73. Peeters, J. G. C. *et al*. Inhibition of Super-Enhancer Activity in Autoinflammatory Site-Derived T Cells Reduces Disease-Associated Gene Expression. *Cell Rep*. **12**, 1986–1996 (2015).

74. Vicente, C. *et al*. The CCR4-NOT complex is a tumor suppressor in Drosophila melanogaster eye cancer models. *J. Hematol. Oncol*. (2018) doi:10.1186/s13045-018-0650-0.

75. Weißbach, S. *et al*. The molecular spectrum and clinical impact of DIS3 mutations in multiple myeloma. *Br. J. Haematol*. (2015) doi:10.1111/bjh.13256.

76. Desterke, C., Bennaceur-Griscelli, A. & Turhan, A. G. DIS3 Mutation in RUNX1-Mutated AML1 Confers a Highly Dismal Prognosis in AML By Repressing Sister Chromatid Cohesion. *Blood* (2019) doi:10.1182/blood-2019-123352.

77. Aghib, D. F. & Bishop, J. M. A 3' truncation of myc caused by chromosomal translocation in a human T-cell leukemia is tumorigenic when tested in established rat fibroblasts. *Oncogene* **6**, 2371–5 (1991).

78. Aghib, D. F. *et al*. A 3' truncation of MYC caused by chromosomal translocation in a human T-cell leukemia increases mRNA stability. *Oncogene* **5**, 707–11 (1990).

79. Xia, Z. *et al*. Dynamic analyses of alternative polyadenylation from RNA-seq reveal a 3'2-UTR landscape across seven tumour types. *Nat. Commun*. **5**, (2014).

80. Yuan, F., Hankey, W., Wagner, E. J., Li, W. & Wang, Q. Alternative polyadenylation of mRNA and its role in cancer. *Genes Dis*. **8**, 61–72 (2021).

81. Pereira, B., Billaud, M. & Almeida, R. RNA-Binding Proteins in Cancer: Old Players and New Actors. *Trends in Cancer* (2017) doi:10.1016/j.trecan.2017.05.003.

82. Mohibi, S., Chen, X. & Zhang, J. Cancer the'RBP'eutics–RNA-binding proteins as therapeutic targets for cancer. *Pharmacology and Therapeutics* (2019) doi:10.1016/j.pharmthera.2019.07.001.

83. Meisner, N. C. *et al*. Identification and mechanistic characterization of low-molecular-weight inhibitors for HuR. *Nat. Chem. Biol*. (2007) doi:10.1038/nchembio.2007.14.

84. Huang, M. *et al*. DbCoRC: A database of core transcriptional regulatory circuitries modeled by H3K27ac ChIP-seq signals. *Nucleic Acids Res*. **46**, D71–D77 (2018).

85. Wu, M. *et al*. The RNA exosome shapes the expression of key protein-coding genes. *Nucleic Acids Res*. 1–20 (2020) doi:10.1093/nar/gkaa594.

1. Bradner, J. E., Hnisz, D. & Young, R. A. Transcriptional Addiction in Cancer. *Cell* **168**, 629–643 (2017).

2. Bywater, M. J., Pearson, R. B., Mcarthur, G. A. & Hannan, R. D. Dysregulation of the basal RNA polymerase transcription apparatus in cancer. *Nat. Rev. Cancer* **13**, (2013).

3. Villicaña, C., Cruz, G. & Zurita, M. The basal transcription machinery as a target for cancer therapy. (2014).

4. Laham-karam, N., Pinto, G. P., Poso, A. & Kokkonen, P. Transcription and Translation Inhibitors in Cancer Treatment. **8**, 1–24 (2020).

5. Puissant, A. *et al*. Targeting MYCN in neuroblastoma by BET bromodomain inhibition. *Cancer Discov*. (2013) doi:10.1158/2159-8290.CD-12-0418.

6. Bandopadhayay, P. *et al*. BET bromodomain inhibition of MYC-amplified medulloblastoma. *Clin. Cancer Res*. (2014) doi:10.1158/1078-0432.CCR-13-2281.

7. Lockwood, W. W., Zejnullahu, K., Bradner, J. E. & Varmus, H. Sensitivity of human lung adenocarcinoma cell lines to targeted inhibition of BET epigenetic signaling proteins. *Proc. Natl. Acad. Sci. U. S. A*. (2012) doi:10.1073/pnas.1216363109.

8. Filippakopoulos, P. *et al*. Selective inhibition of BET bromodomains. *Nature* 1–7 (2010) doi:10.1038/nature09504.

9. Abedin, S. M., Boddy, C. S. & Munshi, H. G. BET inhibitors in the treatment of hematologic malignancies: Current insights and future prospects. *OncoTargets and Therapy* (2016) doi:10.2147/OTT.S100515.

10. Asangani, I. A. *et al*. Therapeutic targeting of BET bromodomain proteins in castration-resistant prostate cancer. *Nature* (2014) doi:10.1038/nature13229.

11. Chaidos, A. *et al*. Potentantimyeloma activity of the novel bromodomain inhibitors I-BET151 and I-BET762. *Blood* (2014) doi:10.1182/blood-2013-01-478420.

12. Winter, G. E. *et al*. Phthalimide conjugation as a strategy for in vivo target protein degradation. *Science (80-.).* **348**, 1376–1382 (2015).

13. Chung, C., Chandwani, R., Marazzi, I., Wilson, P. & Coste, H. Suppression of inflammation by a synthetic histone mimic. *Nature* **468**, 1119–1123 (2017).

14. Lasko, L. M. *et al*. Discovery of a selective catalytic p300/CBP inhibitor that targets lineage-specific tumours. *Nature* **550**, 128–132 (2017).

15. Galbraith, M. D., Bender, H. & Espinosa, J. M. Therapeutic targeting of transcriptional cyclin-dependent kinases. *Transcription* **10**, 118–136 (2019).

16. Bensaude, O. Inhibiting eukaryotic transcription: Which compound to choose? How to evaluate its activity? *Transcription* **2**, 103–108 (2011).

17. Baker, A. *et al*. The CDK9 inhibitor dinaciclib exerts potent apoptotic and antitumor effects in preclinical models of MLL-rearranged acute myeloid Leukemia. *Cancer Res*. (2016) doi:10.1158/0008-5472.CAN-15-1070.

18. Gregory, G. P. *et al*. CDK9 inhibition by dinaciclib potently suppresses Mcl-1 to induce durable apoptotic responses in aggressive MYC-driven B-cell lymphoma in vivo. *Leukemia* (2015) doi:10.1038/leu.2015.10.

19. Martin, R. D., Hébert, T. E. & Tanny, J. C. Therapeutic targeting of the general RNA polymerase II transcription machinery. *Int. J. Mol. Sci.* **21**, (2020).

20. Jia, Q., Chen, S., Tan, Y., Li, Y. & Tang, F. Oncogenic super-enhancer formation in tumorigenesis and its molecular mechanisms. *Exp. Mol. Med.* **52**, 713–723 (2020).

21. Lovén, J. *et al*. Selective inhibition of tumor oncogenes by disruption of super-enhancers. *Cell* (2013) doi:10.1016/j.cell.2013.03.036.

22. Chipumuro, E. *et al*. CDK7 inhibition suppresses super-enhancer-linked oncogenic transcription in MYCN-driven cancer. *Cell* **159**, 1126–1139 (2014).

23. Christensen, C. L. *et al*. Targeting Transcriptional Addictions in Small Cell Lung Cancer with a Covalent CDK7 Inhibitor. *Cancer Cell* (2014) doi:10.1016/j.ccell.2014.10.019.

24. Kwiatkowski, N. *et al*. Targeting transcription regulation in cancer with a covalent CDK7 inhibitor. *Nature* **511**, 616–620 (2014).

25. Laitem, C. *et al*. CDK9 inhibitors define elongation checkpoints at both ends of RNA polymerase II-transcribed genes. *Nat. Struct. Mol. Biol.* **22**, 396–403 (2015).

26. Herzog, V. A. *et al*. Thiol-linked alkylation of RNA to assess expression dynamics. *Nat. Methods* **14**, 1198–1204 (2017).

27. Lusser, A. *et al*. Thiouridine-to-Cytidine Conversion Sequencing (TUC-Seq) to Measure mRNA Transcription and Degradation Rates. *Methods Mol. Biol.* (2020) doi:10.1007/978-1-4939-9822-7_10.

28. Schofield, J. A., Duffy, E. E., Kiefer, L., Sullivan, M. C. & Simon, M. D. TimeLapse-seq: Adding a temporal dimension to RNA sequencing through nucleoside recoding. *Nat. Methods* **15**, 221–225 (2018).

29. Michel, M., Zacher, B., Demel, C., Tresch, A. & Gagneur, J. TT-seq maps the human transient transcriptome. *Science (80-.).* **352**, (2016).

30. Rabani, M. *et al*. Metabolic labeling of RNA uncovers principles of RNA production and degradation dynamics in mammalian cells. *Nat. Biotechnol.* **29**, (2011).

31. Duffy, E. E. *et al*. Tracking Distinct RNA Populations Using Efficient and Reversible Covalent Chemistry Technology Tracking Distinct RNA Populations Using Efficient and Reversible Covalent Chemistry. *Mol. Cell* **59**, 858–866 (2015).

32. Muhar, M. *et al*. SLAM-seq defines direct gene-regulatory functions of the BRD4-MYC axis. *Science (80-.).* **360**, 800–805 (2018).

33. Mertz, J. A. *et al*. Targeting MYC dependence in cancer by inhibiting BET bromodomains. *Proc. Natl. Acad. Sci. U. S. A.* **108**, 16669–16674 (2011).

34. Parua, P. K. *et al*. A Cdk9-PP1 switch regulates the elongation-termination transition of RNA polymerase II. *Nature* **558**, 460–464 (2018).

35. Alexander J. Federation, Donald R. Polaski, C. J. O., Fan, A., Lin, C. Y., E., J. & Bradner. Identification of candidate master transcription factors within enhancer-centric transcriptional regulatory networks. *bioRxiv* (2018).

36. Yamada, T. & Akimitsu, N. Contributions of regulated transcription and mRNA decay to the dynamics of gene expression. *Wiley* 1–18 (2019) doi:10.1002/wrna.1508.

37. Wu, Q. *et al*. Translation affects mRNA stability in a codon-dependent manner in human cells. *Elife* 1–22 (2019).

38. Hnisz, D. *et al*. Super-enhancers in the control of cell identity and disease. *Cell* (2013) doi:10.1016/j.cell.2013.09.053.

39. Zuber, J. *et al*. RNAi screen identifies Brd4 as a therapeutic target in acute myeloid leukaemia. *Nature* **478**, 524–528 (2011).

40. Delmore, J. E. *et al*. BET bromodomain inhibition as a therapeutic strategy to target c-Myc. *Cell* **146**, 904–917 (2011).

41. Dawson, M. A. *et al*. Inhibition of BET recruitment to chromatin as an effective treatment for MLL-fusion leukaemia. *Nature* **478**, 529–533 (2011).

42. Chen, J., Xu, H., Aronow, B. J. & Jegga, A. G. Improved human disease candidate gene prioritization using mouse phenotype. *BMC Bioinformatics* **8**, 1–13 (2007).

43. Chen, J., Aronow, B. J. & Jegga, A. G. Disease candidate gene identification and prioritization using protein interaction networks. *BMC Bioinformatics* **10**, 1–14 (2009).

44. Chen, J., Bardes, E. E., Aronow, B. J. & Jegga, A. G. ToppGene Suite for gene list enrichment analysis and candidate gene prioritization. *Nucleic Acids Res*. **37**, 305–311 (2009).

45. Zhou, Y. *et al*. Metascape provides a biologist-oriented resource for the analysis of systems-level datasets. *Nat. Commun*. (2019) doi:10.1038/s41467-019-09234-6.

46. Gilan, O. *et al*. Selective targeting of BD1 and BD2 of the BET proteins in cancer and immunoinflammation. *Science (80-.)*. **368**, 387–394 (2020).

47. Timmers, H. T. M. & Tora, L. Transcript Buffering: A Balancing Act between mRNA Synthesis and mRNA Degradation. *Mol. Cell* **72**, 10–17 (2018).

48. Ye, C. *et al*. DRUG-seq for miniaturized high-throughput transcriptome profiling in drug discovery. *Nat. Commun*. 1–9 (2018) doi:10.1038/s41467-018-06500-x.

49. Chen, C. Y. A. & Shyu, A. Bin. AU-rich elements: characterization and importance in mRNA degradation. *Trends in Biochemical Sciences* (1995) doi:10.1016/S0968-0004(00)89102-1.

50. Grzybowska, E. A., Wilczynska, A. & Siedlecki, J. A. Regulatory Functions of 3′UTRs. *Biochem. Biophys. Res. Commun*. (2001) doi:10.1006/bbrc.2001.5738.

51. Lal, A. *et al*. miR-24 Inhibits Cell Proliferation by Targeting E2F2, MYC, and Other Cell-Cycle Genes via Binding to 'Seedless' 3′UTR MicroRNA Recognition Elements. *Mol. Cell* **35**, 610–625 (2009).

52. Sachdeva, M. *et al*. p53 represses c-Myc through induction of the tumor suppressor miR-145. *Proc. Natl. Acad. Sci. U. S. A*. **106**, 3207–3212 (2009).

53. Yeilding, N. M., Rehman, M. T. & Lee, W. M. Identification of sequences in c-myc mRNA that regulate its steady-state levels. *Mol. Cell. Biol*. **16**, 3511–3522 (1996).

54. Caput, D. *et al*. Identification of a common nucleotide sequence in the 3'-untranslated region of mRNA molecules specifying inflammatory mediators. *Proc. Natl. Acad. Sci. U. S. A*. (1986) doi:10.1073/pnas.83.6.1670.

55. Kataoka, K. *et al*. Aberrant PD-L1 expression through 3′-UTR disruption in multiple cancers. *Nature* **534**, 402–406 (2016).

56. Buffering, T., Act, B., Synthesis, R. N. A. & Degradation, R. N. A. Transcript Buffering : A Balancing Act between mRNA Synthesis and mRNA Degradation. *Mol. Cell* (2018) doi:10.1016/j.molcel.2018.08.023.

57. Jia, Y., Chng, W. J. & Zhou, J. Super-enhancers: Critical roles and therapeutic targets in

hematologic malignancies. *J. Hematol. Oncol.* **12**, 1–17 (2019).

58. Gryder, B. E. *et al.* Chemical genomics reveals histone deacetylases are required for core regulatory transcription. *Nat. Commun.* **10**, 1–12 (2019).

59. Schwanhüusser, B. *et al.* Global quantification of mammalian gene expression control. *Nature* **473**, 337–342 (2011).

60. Ruzsics, Z., Koszinowski, U. H., Friedel, C. C., Do, L. & Zimmer, R. Conserved principles of mammalian transcriptional regulation revealed by RNA half-life. *Nucleic Acids Res.* **37**, (2009).

61. Alon, U. *An introduction to systems biology: Design principles of biological circuits. An Introduction to Systems Biology: Design Principles of Biological Circuits* (2006).

62. Mayr, C. & Bartel, D. P. Widespread Shortening of 3′UTRs by Alternative Cleavage and Polyadenylation Activates Oncogenes in Cancer Cells. *Cell* **138**, 673–684 (2009).

63. Colley, S. M., Tilbrook, P. A. & Klinken, S. P. Increased transcription of the Eμ-myc transgene and mRNA stabilisation produce only a modest elevation in Myc protein. *Oncogene* **14**, 2735–2739 (1997).

64. Zhu, H. *et al.* BET Bromodomain Inhibition Promotes Anti-Tumor Immunity by Suppressing PD-L1 expression. *Cell Rep.* **16**, 2829–2837 (2017).

65. Hogg, S. J. *et al.* BET-Bromodomain Inhibitors Engage the Host Immune System and Regulate Expression of the. *Cell Rep.* **18**, 2162–2174 (2017).

66. Zhang, H. *et al.* Targeting CDK9 Reactivates Epigenetically Silenced Genes in Cancer. *Cell* **175**, 1244-1258.e26 (2018).

67. Duan, Q. *et al.* BET bromodomain inhibition suppresses innate inflammatory and profibrotic transcriptional networks in heart failure. *Sci. Transl. Med.* **9**, 23–25 (2017).

68. Klein, K. Bromodomain protein inhibition: A novel therapeutic strategy in rheumatic diseases. *RMD Open* **4**, 1–10 (2018).

69. Rossi, A. G. *et al.* Cyclin-dependent kinase inhibitors enhance the resolution of inflammation by promoting inflammatory cell apoptosis. *Nat. Med.* **12**, 1056–1064 (2006).

70. Wang, K. *et al.* Cyclin-dependent kinase 9 activity regulates neutrophil spontaneous apoptosis. *PLoS One* **7**, 3–8 (2012).

71. Hellvard, A. *et al.* Inhibition of CDK9 as a therapeutic strategy for inflammatory arthritis. *Sci. Rep.* **6**, 1–11 (2016).

72. Hogg, S. J., Beavis, P. A., Dawson, M. A. & Johnstone, R. W. Targeting the epigenetic regulation of antitumour immunity. *Nat. Rev. Drug Discov.* **19**, 776–800 (2020).

73. Peeters, J. G. C. *et al.* Inhibition of Super-Enhancer Activity in Autoinflammatory Site-Derived T Cells Reduces Disease-Associated Gene Expression. *Cell Rep.* **12**, 1986–1996 (2015).

74. Vicente, C. *et al.* The CCR4-NOT complex is a tumor suppressor in Drosophila melanogaster eye cancer models. *J. Hematol. Oncol.* (2018) doi:10.1186/s13045-018-0650-0.

75. Weißbach, S. *et al.* The molecular spectrum and clinical impact of DIS3 mutations in multiple myeloma. *Br. J. Haematol.* (2015) doi:10.1111/bjh.13256.

76. Desterke, C., Bennaceur-Griscelli, A. & Turhan, A. G. DIS3 Mutation in RUNX1-Mutated AML1 Confers a Highly Dismal Prognosis in AML By Repressing Sister Chromatid Cohesion. *Blood* (2019) doi:10.1182/blood-2019-123352.

77. Aghib, D. F. & Bishop, J. M. A 3' truncation of myc caused by chromosomal translocation in a human T-cell leukemia is tumorigenic when tested in established rat fibroblasts. *Oncogene* **6**, 2371–5 (1991).

78. Aghib, D. F. *et al*. A 3' truncation of MYC caused by chromosomal translocation in a human T-cell leukemia increases mRNA stability. *Oncogene* **5**, 707–11 (1990).

79. Xia, Z. *et al*. Dynamic analyses of alternative polyadenylation from RNA-seq reveal a 3'2-UTR landscape across seven tumour types. *Nat. Commun.* **5**, (2014).

80. Yuan, F., Hankey, W., Wagner, E. J., Li, W. & Wang, Q. Alternative polyadenylation of mRNA and its role in cancer. *Genes Dis.* **8**, 61–72 (2021).

81. Pereira, B., Billaud, M. & Almeida, R. RNA-Binding Proteins in Cancer: Old Players and New Actors. *Trends in Cancer* (2017) doi:10.1016/j.trecan.2017.05.003.

82. Mohibi, S., Chen, X. & Zhang, J. Cancer the'RBP'eutics–RNA-binding proteins as therapeutic targets for cancer. *Pharmacology and Therapeutics* (2019) doi:10.1016/j.pharmthera.2019.07.001.

83. Meisner, N. C. *et al*. Identification and mechanistic characterization of low-molecular-weight inhibitors for HuR. *Nat. Chem. Biol.* (2007) doi:10.1038/nchembio.2007.14.

84. Huang, M. *et al*. DbCoRC: A database of core transcriptional regulatory circuitries modeled by H3K27ac ChIP-seq signals. *Nucleic Acids Res.* **46**, D71–D77 (2018).

85. Wu, M. *et al*. The RNA exosome shapes the expression of key protein-coding genes. *Nucleic Acids Res.* 1–20 (2020) doi:10.1093/nar/gkaa594.